Physics – Uspekhi **52** (6) 615 – 647 (2009)

ORAL ISSUE OF THE JOURNAL "USPEKHI FIZICHESKIKH NAUK" PACS numbers: **07.35.+k**, **29.20.–c**, **42.62.–b**, **97.60.–s**

Extreme states of matter on Earth and in space

V E Fortov

DOI: 10.3367/UFNe.0179.200906h.0653

Contents

Abstract. This review is concerned with the results of studies into the behavior of substances at ultimately high pressures and temperatures obtainable by way of kinetic or electromagnetic energy cumulation in laboratory conditions. Also considered are the diversified states of matter and the processes occurring under gravitational forces and thermonuclear energy release.

1. Introduction

> *We already know the laws that govern the behavior of matter under all but the most extreme conditions.*
> S Hawking. *A Brief History of Time* (*p. 168*)

The state of matter at extremely high temperatures and densities, and hence with extraordinarily high energy densities, has always attracted researchers due to the possibility of reaching new parameter records, the prospect of advancing to new regions of the phase diagram, and the potentiality of producing in laboratory conditions the exotic states that gave birth to our Universe through the Big Bang and wherein the great bulk (95%) of baryon (visible) matter in nature now resides: in the plasmas of ordinary and neutron stars, pulsars, black holes, and giant planets, as well as in the multitude of planets, including those discovered quite recently. Prior to becoming a star, matter in the Universe experiences a succession of diverse physical transformations: from quarks and bosons to complex molecules and again to atoms and particles; from relativistic energies to absolute zero and again to the state of high-energy dense plasma, and from enormous densities to ultrahigh vacuum and again to the densities of the atomic nucleus and quarks. And so our fundamental knowledge about the structure, evolution, and history of the Universe is directly dependent on an understanding of the behavior of matter in all of its transformations up to its transition to ultrahigh energy density states, which forms not only specific physical models, but also the worldview of modern natural science. Only by steadily increasing the high energy densities attainable through investigations on Earth and in space may we delve into the past, as if using a time machine, looking for the singular conditions of the Big Bang — the instant of the Universe's inception ~ 15 billion years ago [1 – 10].

Furthermore, a stable pragmatic incentive to pursue suchlike investigations is the practical application of extreme states in nuclear, thermonuclear, and pulsed energetics, as well as in high-voltage and high-power electrophysics, and for the synthesis of superhard materials, for strengthening and welding materials, for the impact protection of space vehicles, and, of course, in the field of defense — because the operation of nuclear devices with controllable (inertial controlled thermonuclear fusion, ICTF) and quasicontrollable (atomic and hydrogen bombs) energy release relies on the initiation of nuclear reactions in a strongly compressed and heated nuclear fuel.

V E Fortov Institute of the Thermophysics of Extreme States,
Joint Institute for High Temperatures, Russian Academy of Sciences
ul. Izhorskaya 13/19, 125412 Moscow, Russian Federation
Tel. (7-495) 484-23 00, (7-495) 483 23 14
Fax (7-495) 485 79 90
E-mail: fortov@ras.ru; fortov@ihed.ras.ru

Received 10 November 2008
Uspekhi Fizicheskikh Nauk **179** (6) 653 – 687 (2009)
DOI: 10.3367/UFNr.0179.200906h.0653
Translated by E N Ragozin; edited by A Radzig

The revolutionary discoveries in astronomy (neutron stars, pulsars, black holes, γ-ray bursts, exoplanets, etc.) of the last decades [1, 5 – 10] furnish new examples of extreme states, which call for investigation in order to solve the fundamental problems of modern astrophysics.

The application of highly sophisticated high-power energy cumulation systems: chemical and nuclear explosives; powder, light-gas, and electrodynamic 'guns'; charged-particle fluxes; laser and X-ray radiation, as well as relativistic ion streams has enabled, since the time of the battle between David and Goliath, raising the throwing speed of a macroscopic striker by three–four orders of magnitude and the pressure in a shock wave by six–eight orders of magnitude, thereby attaining the megabar–gigabar pressure range and the 'nuclear' energy densities in substances.

The use of high-frequency electromagnetic fields for the electrodynamic acceleration of charged particles to near-luminal speeds ($v/c \approx 0.999999991$) makes it possible to realize in head-on collisions ultrahigh energy densities of $1.6 \times 10^{29} - 1.6 \times 10^{30}$ J cm^{-3} (1 – 10 GeV fm^{-3}) and a pressure of order 10^{30} bar, which are sufficient for quark deconfinement and the emergence of quark–gluon plasma, as well as maybe the production of Higgs bosons. These ultrahigh energy densities, which existed only several microseconds after the first instant of the Big Bang, are leading researchers to the frontiers of modern physics.

The development of the physics of extremely high energy densities is largely determined by the implementation of defense, space, and nuclear programs in which extremely high pressures and temperatures are the elements required for directional action on substances and the initiation of nuclear reactions in compressed and heated nuclear fuel. At the same time, the range of technical applications related to the physics of extreme states is broadening constantly. These states of matter underlie the operation of pulsed thermonuclear reactors with the inertial confinement of hot plasma, high-power magnetohydrodynamic and explosive magnetic generators, power installations and rocket propulsors with gas-phase nuclear reactors, plasmachemical and microwave reactors, plasmatrons, and high-power sources of optical and X-ray radiation. Extreme states emerge when a substance is subjected to intense shock, detonation, and electroexplosion waves, concentrated laser radiation, and electron and ion beams, as well as in powerful chemical and nuclear explosions, in the pulsed vaporization of liners in pinches and magnetic cumulation generators, in the hypersonic motion of bodies in dense planetary atmospheres, in high-velocity impacts, and in many other situations characterized by ultimately high pressures and temperatures. The physics of near-electrode, contact, and electroexplosion processes in a vacuum breakdown is intimately related to the high-energy plasma which determines the operation of high-power pulsed accelerators, microwave radiation generators, and plasma switches. This list can easily be extended.

High energy density physics has been making rapid strides due to the advent of new devices for the generation of high energy densities, like relativistic ion accelerators, lasers, high-current Z-pinches, explosive and electroexplosion generators of intense shock waves, multistage light-gas guns, and diamond anvils. These complex and expensive technical devices have made it possible to substantially advance along the scale of energy density attainable in a physical experiment and to obtain in laboratory or quasilaboratory conditions the macroscopic volumes of matter in states that range into the megabar–gigabar pressure region unattainable with the traditional techniques of experimental physics. The employment of new generators for the cumulation of high energy densities leads to a variety of fascinating physical effects, like a radical restructuring of the energy spectrum and composition of a compressed and heated material [1 – 5, 11], new cooperative effects and the development of diverse instabilities in the interaction of directed energy fluxes with a dense plasma, its unsteady motion under the conditions of substantial radiative energy transfer, relativistic, gravitational, and nuclear phenomena, as well as a number of other exotic effects which may now be predicted, if at all, only in the most general form [5 – 7].

Recently, interest in the science of extreme states has also been rekindled due to the emergence of new intriguing astrophysical data obtained by modern-generation ground-based and space telescopes with different wavelengths and unmanned space stations.

Although the upper limit on pressure in laboratory plasmas so far differs from the maximum astrophysical value by 20 – 30 orders of magnitude, this gap is rapidly shrinking. The physical processes in a laboratory and in space quite frequently exhibit an amazing diversity and, at the same time, a deep analogy, thereby testifying, at the least, to the uniformity of the physical principles of the behavior of matter over extremely broad ranges of pressure (42 orders of magnitude) and temperature (up to 10^{21} K).

Today we can clearly see that the study of matter in extreme states is one of the 'hottest' and most rapidly developing basic scientific disciplines which are at the interface between plasma physics, condensed-matter physics, nuclear, atomic, and molecular physics, nonlinear optics, and relativistic and magnetic hydrodynamics, involving a wealth of compression- and heating-stimulated physical effects and a permanently widening variety of objects and states in which the plasma nonideality plays a crucial role. Despite the extraordinary diversity of the objects and experimental and astrophysical situations, they all share the common trait, that of a decisive role played by high energy densities in their physical behavior.

It is no accident that half of the 30 problems of "the physics minimum at the beginning of the XXIst century" proposed by Academician V L Ginzburg [5] are to a greater or lesser degree dedicated to high energy density physics.

These circumstances are a permanent steadfast stimulus to intensive theoretical and experimental investigations which have recently resulted in a great body of new and, above all, reliable information about the thermodynamic, structural, gas-dynamic, optical, electrophysical, and transport properties of matter under extreme conditions. These specific data are contained in a massive flow of original publications and reports at conferences, a part of which are not easily accessible to Russian scientists.

The term 'high' is conventionally [1 – 5, 9] used in reference to in-substance energy densities exceeding approximately $10^4 - 10^5$ J cm^{-3}, which corresponds to the binding energy of condensed media (for instance, explosives, H_2, or metals) and a pressure level of a few millions of atmospheres.

As a rule, a substance under high energy density conditions resides in the plasma state — an ionized state — due to thermal and/or pressure-induced ionization. In astrophysical objects, such compression and heating are effected by gravitational forces and nuclear reactions, and in laboratory conditions by intense shock waves which are

excited by a wide variety of 'drivers' ranging from two-stage gas guns [12] to lasers [13, 14] and high-current Z-pinches [15, 16] reaching hundreds of terawatts of power.[1] However, while the lifetime of extreme states in astrophysical objects ranges from milliseconds to billions of years, making it possible to conduct their detailed observation and measurement with the help of space probes and orbital and ground-based telescopes, in terrestrial conditions we have to make do with the microsecond–femtosecond duration range [2 – 4, 14], which calls for the application of ultimately fast specific diagnostic techniques.

At present, every large-scale physical facility which generates extremely high pressures and temperatures is engaged in work programs (not infrequently international) on the fundamental physics of high energy density, apart from having pragmatic-dedicated tasks in pulsed energetics or defense. It is significant that the experimental capabilities of impulse technologies broaden rapidly and encroach on the province of the megabar–gigabar range. Supplemented by the data obtained in experiments with diamond anvils, explosion and electroexplosion devices, and light-gas guns, these record parameters are now the source of new and quite often unexpected information about the behavior of plasmas with extreme parameter values [3, 4].

Interestingly, when conducting experiments on extreme-state laboratory plasmas, even today it is possible to partly reproduce on a small scale many parameters of astrophysical objects and the effects and processes occurring therein, the information on which has become accessible due to the use of ground- and space-based observation facilities. These are the data on hydrodynamic mixing and instabilities, shock-wave phenomena, strongly radiating and relativistic streams and jets, solitons, relativistic phenomena, equations of state, the composition and spectra of compressed nonideal plasmas, and the characteristics of interstellar cosmic plasma, dust, etc.

The distinguishing features of high energy density physics are an extreme complexity and strong nonlinearity of the plasma processes covered by it, the significance of collective interparticle interaction, and relativity. This makes the study of phenomena occurring in this area a fascinating and absorbing task which continually attracts new researchers.

All things considered, the National Research Council (NRC) of the US National Academy of Sciences formulated a large-scale national program of research [5] in the field of high energy density physics and gave it a high priority. Similar work programs are being vigorously pursued in many developed countries capable of making the requisite experimental facilities and having the relevant qualified personnel.

In this report an attempt is made to systematize, generalize, and set forth from a unified viewpoint the experimental and theoretical material relating to this new realm of science and to show, following Titus Lucretius Carus, "Thus from the mixture of the elements there emerge infinite multitudes of creatures, which are strange and highly diversified in appearance" [17]. In doing this, the author endeavored to discuss the maximally broad range of problems related to precisely the high energy density physics. That is why many interesting astrophysical, laser, and nuclear-physical problems, as well as technical applications, are outlined only briefly, but as the text goes the reader is referred to original papers and monographs where these issues are considered at length. Since one report cannot encompass everything known about extreme states of matter to date, the emphasis was placed on those issues which appeared to be the most interesting to the author and which he happened to directly work on.

Owing to the extensiveness and heterogeneity of the material, the exposition will in some cases be inherently lapidary and will be attended with references to specialized reviews and monographs [1 – 10, 18 – 34].

[1] The total power of terrestrial electric power plants amounts to about 3.5 TW.

2. Matter under extreme conditions. Classification of states

Figure 1 shows the schematic diagram of extreme states of matter, which are realized in a number of natural objects and in laboratory or quasilaboratory conditions.

The emergence of extreme states in nature is caused by the gravitational forces, which are inherently long-range and unscreened, unlike Coulomb forces (in plasmas). These forces compress and heat the substance either directly or by additionally stimulating exothermic nuclear reactions in massive astrophysical objects [1, 6, 7].

The scale range of extreme states realized in nature is capable of defying the most vivid imagination (Figs 1b and 1c). At the bottom of the Mariana Trough (11 km in depth), the water pressure amounts to 1.2 kbar; at the Earth's center the pressure is $p \sim 3.6$ Mbar, the temperature $T \sim 0.5$ eV, and the density $\rho \sim 10-20$ g cm^{-3}; at the center of Jupiter $p \sim 40-60$ Mbar, $\rho \sim 30$ g cm^{-3}, $T \sim 2 \times 10^4$ K; at the center of the Sun $p \sim 240$ Gbar, $T \sim 1.6 \times 10^3$ eV, $\rho \sim 150$ g cm^{-3}; in stars that are cooling down, known as white dwarfs, $p \sim 10^{10}-10^{16}$ Mbar, $\rho \sim 10^6-10^9$ g cm^{-3}, and $T \sim 10^3$ eV. In targets for controlled fusion with inertial plasma confinement $p \sim 200$ Gbar, $\rho \sim 150-200$ g cm^{-3}, and $T \sim 10^8$ eV. Neutron stars, which are elements of pulsars, black holes, γ-ray bursts, and magnetars, supposedly have the record-high parameters: $p \sim 10^{19}$ Mbar, $\rho \sim 10^{11}$ g cm^{-3}, $T \sim 10^4$ eV for the mantle, and $p \sim 10^{22}$ Mbar, $\rho \sim 10^{14}$ g cm^{-3}, $T \sim 10^4$ eV for the core with a giant magnetic field of $10^{11}-10^{16}$ G.

As noted in the Introduction, by the lower bound of 'high energy densities' we imply an energy density of 10^4-10^5 J cm^{-3}, comparable to the binding energy of condensed matter, which corresponds to the valence electron binding energy (of several electron-volts) and to pressures of order 100 kbar – 1 Mbar. These pressures far exceed the ultimate mechanical strength of materials and call for taking account of their compressibility and, hence, of hydrodynamic motion under pulsed energy release.

In the regions of low pressure and temperature, matter occurs in those exceptionally diverse molecular and structural forms in which we encounter it at normal conditions day after day [1]. The physical, chemical, structural, and biological properties of substances are sharp nonmonotonic functions of the nuclear charge and elemental composition. These properties are determined by the details and peculiarities of location of the electron energy levels in atoms, ions, and molecules, which eventually underlies the amazing diversity of the forms and manifestations of the surrounding living and inorganic nature on the Earth. These features are to a certain extent reflected in the Periodic Table of elements.

With an increase in energy density (p and T), substances acquire an increasingly universal — self-similar — structure

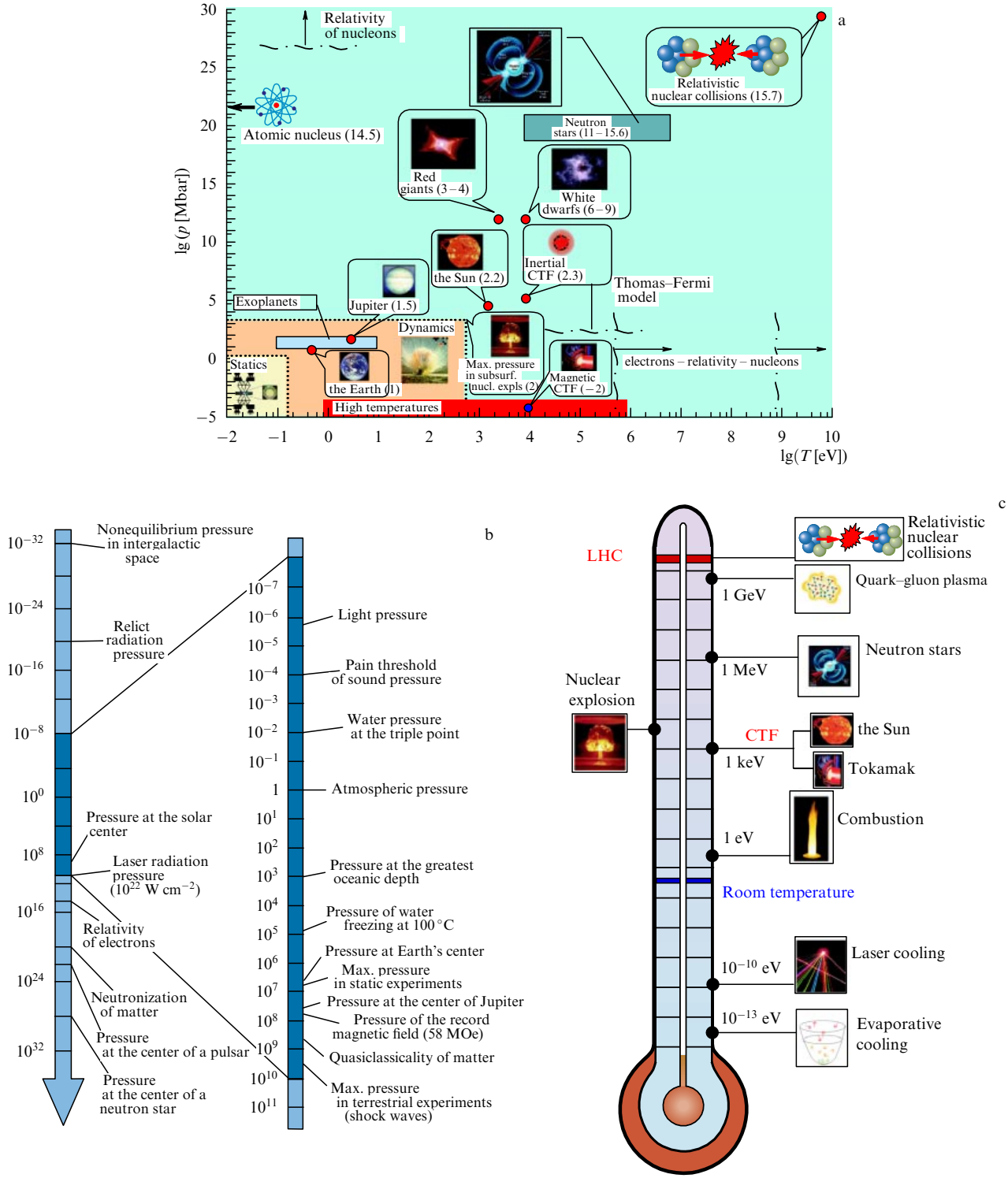

Figure 1. (a)Extreme states [1] in nature and in the laboratory. The figures in parentheses indicate the logarithm of density (in g cm^{-3}). The domains called 'Statics' and 'Dynamics' corresponds to static and dynamic techniques for high-pressure production, and 'High temperatures' to high-temperature experiments. (b) The pressure scale range (1 atm $\approx 10^5$ Pa) in nature encompasses 64 orders of magnitude. The right-hand side of the scale relates to experimentally attainable conditions [18]. (c) Temperature scale.

[1, 2]. The growth in pressure and temperature ruptures molecular complexes to form atomic states. Due to thermal and/or pressure-induced ionization, atomic states next lose outer shell electrons which are responsible for the chemical bonds. Atomic and ion electron shells are restructured to acquire an increasingly regular level occupation, and a crystal lattice after a number of polymorphic transitions (this ordinarily takes place for $p < 0.5$ Mbar) transforms to a close-packed body-centered cubic structure.

These processes of substance property 'simplification' take place when the characteristic energy density comes to be on the order of valence shell energies and amounts to $e^2/a_B^4 \sim 3 \times 10^{14}$ erg cm^{-3} (where $a_B = \hbar^2/(me^2) \approx 5.2 \times 10^{-9}$ cm is the Bohr radius) [1, 2], which determines

the order of magnitude of the substance 'universalization' lower bound: $T \sim 10$ eV, $p \sim 300$ Mbar. The quantitative position of universalization bounds depends on the specific substance and their experimental determination is an important task for high energy density physics, the more so as the theory [19] predicts a highly varied behavior of substances in the ultramegabar pressure range: shell effects [19], electron and plasma phase transitions [20, 21, 35–44], and so forth.

The upper boundary of the domain of extreme states of matter is determined by the contemporary level of knowledge of high-energy physics [7, 10, 45, 46] and observational astrophysical data, and is supposedly limited only by our imagination. The ultraextreme parameters of matter accessible to contemporary physical notions are defined by the so-called Planck quantities [7, 45, 46], which are combinations of the fundamental physical constants: the Planck constant $\hbar$, the speed of light c, the gravitation constant G, and the Boltzmann constant k_B:

the length $l_P = \sqrt{\dfrac{\hbar G}{c^3}} = \dfrac{\hbar}{m_p}\, c = 1.62 \times 10^{-33}$ cm;

the mass (the so-called 'maximon' mass)

$$m_P = \sqrt{\frac{\hbar c}{G}} = 2.18 \times 10^{-5} \text{ g};$$

the time $t_P = \dfrac{l_P}{c} = \dfrac{\hbar}{m_P c^2} = \sqrt{\dfrac{\hbar G}{c^5}} = 5.39 \times 10^{-44}$ s;

the temperature $T_P = \dfrac{m_P c^2}{k_B} = \sqrt{\dfrac{\hbar c^5}{G k_B^2}} = 1.42 \times 10^{32}$ K;

the energy $\mathcal{E}_P = m_P c^2 = \dfrac{\hbar}{t_P} = \sqrt{\dfrac{\hbar c^5}{G}} = 1.96 \times 10^9$ J;

the density $\rho_P = \dfrac{m_P}{l_P^3} = \dfrac{\hbar t_P}{l_P^5} = \dfrac{c^5}{\hbar G^2} = 5.16 \times 10^{93}$ g cm^{-3};

the force $F_P = \dfrac{\mathcal{E}_P}{l_P} = \dfrac{\hbar}{l_P t_P} = \dfrac{c^4}{G} = 1.21 \times 10^{44}$ N;

the pressure $p_P = \dfrac{F_P}{l_P^2} = \dfrac{\hbar}{l_P^3 t_P} = \dfrac{c^7}{\hbar G^2} = 4.63 \times 10^{113}$ Pa;

the charge $q_P = \sqrt{4\pi\varepsilon_0 \hbar c} = 1.78 \times 10^{-18}$ C;

the power $P_P = \dfrac{\mathcal{E}_P}{t_P} = \dfrac{\hbar}{t_P^2} = \dfrac{c^5}{G} = 3.63 \times 10^{52}$ W;

the electric current $I_P = \dfrac{q_P}{t_P} = \sqrt{\dfrac{4\pi\varepsilon_0 c^6}{G}} = 3.48 \times 10^{25}$ A;

the voltage $V_P = \dfrac{\mathcal{E}_P}{q_P} = \dfrac{\hbar}{t_P} = \sqrt{\dfrac{c^4}{4\pi\varepsilon_0 G}} = 1.05 \times 10^{27}$ V;

the electric field strength

$$E_P = \frac{V_P}{l_P} = \frac{1}{G}\sqrt{\frac{c^7}{4\pi\varepsilon_0 \hbar}} = 6.4 \times 10^{59} \text{ V cm}^{-1}, \text{ and}$$

the magnetic field strength

$$H_P = \frac{1}{G}\sqrt{\frac{4\pi\varepsilon_0 c^9}{\hbar}} = 2.19 \times 10^{60} \text{ A m}^{-1} = 1.74 \times 10^{62} \text{ Oe}.$$

These superextreme parameters of matter, at which the known physical laws are supposedly no longer valid, might be realized early in the Big Bang or at the singularity in the collapse of black holes. Discussed in this domain are the physical models assuming that our space has more than three spatial dimensions and that ordinary substance resides in a three-dimensional manifold — in the '3-brane world' [47] embedded in this multidimensional space.

For the present, the capabilities of modern experiments in the field of high energy density physics are far from these 'Planck' values and allow elucidating the properties of elementary particles up to the energies of 0.1–10 TeV and down to distances of 10^{-16} cm. The launch of the Large Hadron Collider (LHC) at CERN has been an important milestone, making attainable the teraelectron-volt energy range.

If we do not fall [1] outside the energy range $mc^2 \sim 1$GeV, which is nonrelativistic for nucleons, we are led to a boundary temperature of 10^9 eV, an energy density of 10^{37} erg cm^{-2}, and a pressure of order 10^{25} Mbar, although it is not unlikely that even more extreme states of matter were realized in the cores of neutron and quark stars and early in the evolution (at nano- and microsecond stages) of the Universe.

Although our experimental capabilities are making rapid strides, they are of course able to only partly encroach on the province of extreme astrophysical states.

Wearing the garland of laurel now are dynamic techniques [2–4, 11, 12, 35, 36, 42] which rely on the pulsed cumulation of high energy densities in substances. The lifetime of such high-energy states is determined by the time of inertial plasma expansion, which typically ranges from 10^{-10} to 10^{-6} seconds and calls for the application of fast sophisticated diagnostic facilities. Table 1 gives the physical conditions corresponding to the lower boundary of the domain of states of interest [3–5, 30]. One can see that the production of high energy densities in plasmas imposes highly demanding requirements on the generation facilities, necessitating efficient spatial and temporal power compression.

Being the most widespread state of matter in nature (98 % of the mass of the Universe, neglecting dark matter), plasma occupies virtually all regions of the phase diagram. In this case, presenting special difficulties in the physical description of such a medium is the nonideal plasma domain, where the Coulomb interparticle interaction energy $e^2 n^{1/3}$ is comparable to or higher than the kinetic energy E_k of particle motion. In this domain, the plasma nonideality parameter $\Gamma = e^2 n^{1/3}/E_k > 1$, and therefore plasma nonideality effects cannot be described by the perturbation theory [1, 3, 4], while the application of numerical parameter-free Monte Carlo or molecular dynamics methods [20, 41] is fraught with the difficulties of selection of adequate pseudopotentials and correct evaluation of quantum effects.

The electron relativity effects in the equation of state and transport plasma properties for the case of $m_e c^2 \approx k_B T$ correspond to $T \approx 0.5$ MeV (6×10^6 K). Above this tem-

Table 1. Physical parameters and conditions corresponding to high energy densities ($10^4 - 10^5$ J cm^{-3}) [5].

Physical conditions and parameters	Parameter values
Energy density W Pressure p	$\sim 10^4 - 10^5$ J cm^{-3} $\sim 0.1 - 1$ Mbar
Condensed explosives: energy density pressure temperature density velocity of detonation	 $\sim 10^4$ J cm^{-3} ~ 400 Kbar ~ 4000 K ~ 2.7 g cm^{-3} $\sim 9 \times 10^5$ cm s^{-1}
Impact of aluminium plate on aluminium: velocity Impact of molybdenum plate on molybdenum: velocity	$(5 - 13.2) \times 10^5$ cm s^{-1} $(3 - 7.5) \times 10^5$ cm s^{-1}
Electromagnetic radiation, laser, intensity q ($W \sim q$), blackbody temperature T ($p \sim T^4$)	$2.6 \times 10^{15} - 3 \times 10^{15}$ W cm^{-2} $2 \times 10^2 - 4 \times 10^2$ eV
Electric field intensity E ($W \sim E^2$) Magnetic field induction B ($W \sim B^2$)	$0.5 \times 10^9 - 1.5 \times 10^9$ V cm^{-1} $1.6 \times 10^2 - 5 \times 10^2$ T
Plasma density n for a temperature $T = 1$ keV ($p = nk_BT$)	$6 \times 10^{19} - 6 \times 10^{20}$ cm^{-3}
Laser radiation intensity q, $\lambda = 1$ μm, $W \sim q^{2/3}$	$0.86 \times 10^{12} - 4 \times 10^{12}$ W cm^{-2}
Blackbody temperature T ($p \sim T^{3.5}$)	66 – 75 eV

perature, matter becomes unstable against spontaneous electron–positron pair production.

Quantum effects are governed by the degeneracy parameter $n\hat{\lambda}^3$ [$\hat{\lambda} = (\hbar^2/2mk_BT)^{1/2}$ is the thermal de Broglie wavelength]. For a degenerate plasma with $n\hat{\lambda}^3 > 1$, the kinetic energy scale is the Fermi energy $E_F \sim \hbar^2 n^{2/3}/2m$, which increases with plasma number density n, making the plasma more and more ideal as it is compressed, $n \to \infty$: $\Gamma = me^2/(\hbar^2 n^{1/3}) \to 0$. The relativity condition, which corresponds to the condition $m_e c^2 \approx E_F \approx 0.5$ MeV, yields a density of order 10^6 g cm^{-3}.

Similar asymptotics also exist in the other limiting case, viz. for a classical ($n\hat{\lambda}^3 \ll 1$) plasma for low $T \to 0$, where $E_k \approx k_BT$ and the plasma becomes increasingly ideal, $\Gamma \sim e^2 n^{1/3}/(k_BT)$, under heating. Therefore, the periphery of the matter phase diagram is occupied by ideal ($\Gamma \ll 1$) Boltzmann ($n\hat{\lambda}^3 \ll 1$) or degenerate ($n\hat{\lambda}^3 > 1$) plasmas which are adequately described by presently elaborated physical models [1 – 4, 20, 37 – 40]. In some cases, attempts to verify these models in dynamic experiments meet with success.

The most significant challenge to the study is presented by the vast domain of nonideal plasmas, $\Gamma \geqslant 1$, occupied by numerous technical applications (semiconductor and metal plasma, pulsed energetics, explosions, arcs, electric discharges, pulsed thermonuclear fusion, etc.) and astrophysical objects like giant planets, exoplanets, brown dwarfs, neutron and quark stars, etc., where the theory predicts qualitatively new physical effects (metallization, 'cold' ionization, dielectrization, plasma phase transitions, etc. [2 – 4, 22]).

Of special interest are plasma phase transitions in strongly nonideal Coulomb systems: the crystallization of dust plasmas [40, 43] and ions in electrostatic traps [44], cyclotrons [48, 49], electrolytes [50, 51], colloidal systems [52], two-dimensional electron systems on the surface of liquid helium [53], exciton condensation in semiconductors, etc. Mention should also be made of the recently discovered phase transition in thermal deuterium plasma [37 – 39, 54] quasia-diabatically compressed to megabar pressures by a series of reverberating shock waves.

The quest for qualitatively new effects of this kind in the nonideal plasma parameter domain is a powerful and permanent incentive to investigate substances at high energy densities [2 – 5].

Another characteristic property of a high-energy-density plasma is the collective nature of its behavior and the strong nonlinearity of response to external energy actions, like shock and electromagnetic waves, solitons, laser radiation, and fast particle fluxes. In particular, the propagation of electromagnetic waves in plasma excites several parametric instabilities (Raman, Thomson, and Brillouin radiation scattering) and is attended by the self-focusing and filamentation of radiation, the development of inherently relativistic instabilities, the production of fast particles and jets, and — at higher intensities — the vacuum 'boiling' with electron–positron pair production [5, 14, 23 – 27, 55 – 61].

In the exposure to extreme energy actions, much attention is given to nonstationary hydrodynamic phenomena, like the instabilities of shock waves and laminar flows [55, 62], jet and soliton dynamics, high-velocity shock (with a Mach number Ma $\approx 15 - 20$), magnetohydrodynamic and radiative (thermal) waves, turbulence, and turbulent mixing in compressible and radiating media [9, 62] (Fig. 2).

All these fascinating and especially nonlinear phenomena manifest themselves both in astrophysical and laboratory plasmas and, despite the enormous difference in spatial scales, have much in common and make up the subject of 'laboratory astrophysics' [9, 60] which permits reproducing in microscopic volumes of matter the states and processes with high energy densities typical for astrophysical objects. Of special value is the information about the equation of state, the composition, optical, and transport properties of plasma, its emission and absorption spectra, cross sections of elementary processes, radiative thermal conductivity coefficients, and properties of relativistic plasma.

Investigations into nonlinear optical effects in circumstances where the interaction of high-power short laser pulses with plasmas occurs enable a major advance in the scales of energy density, specific power, pressure, and temperature by generating extreme-parameter relativistic plasmas in laboratory conditions and attaining in terrestrial conditions the record electric and magnetic intensities, which lead, in particular, to the production of high-energy electron and ion streams [26, 27]. These investigations have already provided a wealth of new information for plasma physics, controlled fusion, and astrophysics, as well as technological and defense applications. The progress of this research may bring into being radically new high-gradient electron accelerators, new sources of high-frequency radiation and light (see Section 4), diagnostic techniques, and novel thermonuclear fusion schemes (see Section 6)

Short-pulse high-power electron beams may generate intense plasma waves which, in combination with ponderomotive forces [26, 27], expel electrons from the plasma channel and produce plasma lenses for energy transport to the center of compressed fusion targets. Furthermore, relativistic electron beams of tremendous peak power emerge inside the plasma under the action of intense intraplasma fields. In particular, with the help of lasers with a petawatt

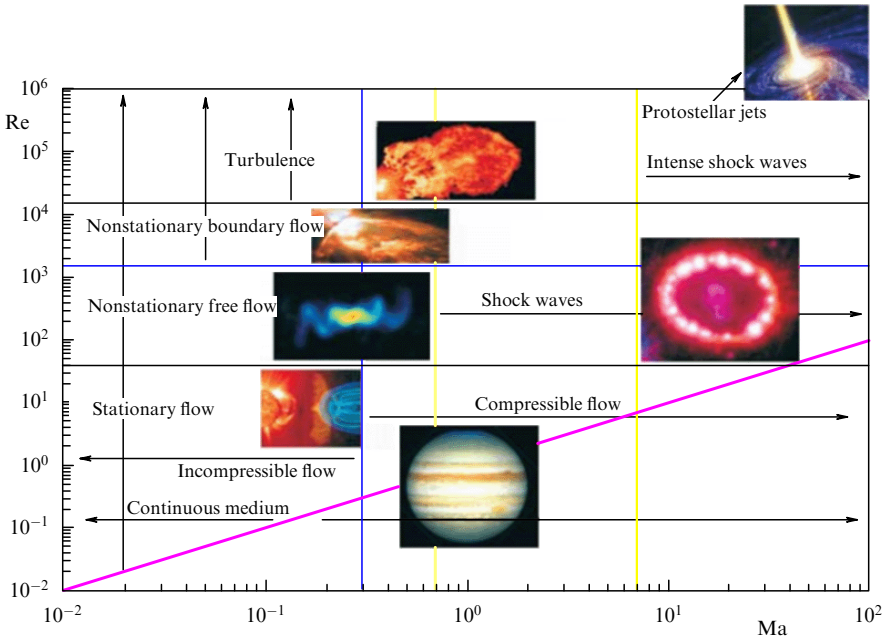

Figure 2. Hydrodynamic modes relating to high energy density physics [5]. In the explosion of an Ia type supernova, the Mach number ranges from 0.01 in the region of thermonuclear combustion to 100 in the shock wave produced by the supernova surface explosion. In the majority of astrophysical phenomena, the Reynolds number Re $> 10^6$ [5].

peak power it has been possible to obtain incredibly high electron and ion currents, which exceed the Alfvén limit by several orders of magnitude, and charged-particle fluxes of the megaelectron-volt energy range [26, 27, 57 – 59].

The interaction of intense electron beams with high-power short laser pulses in turn furnishes the possibility of conducting laboratory experiments in the field of quantum electrodynamics, leading to electron–positron pair production and giving rise to Compton X-ray radiation [26, 27, 61, 63]. This opens up interesting practical opportunities for the development of new-generation compact X-ray sources with record radiation brightness for materials science and medicine.

The generation of high-intensity relativistic electron beams is also attractive as regards their use as the active medium of free-electron lasers. The case in point is 'fourth-generation' X-ray sources with record brightness and tunable wavelength, which is critically important in the pursuance of molecular, biological, and materials technology investigations.

The employment of shock waves generated by sources of locally high energy densities makes it possible to greatly extend the range of experimentally attainable pressures and temperatures and penetrate the parameter domain intermediate between the parameters of chemical explosives and the unique conditions in underground nuclear explosions. Even in the first experiments involving laser-, beam-, and electrodynamically driven shock waves, it was possible to obtain interesting experimental data about the equations of state of hydrogen, deuterium, copper, iron, carbon, and water, and to employ them in the structure analysis of the giant planets of the Solar System and exoplanets [2 – 4, 11, 12, 14 – 16, 22].

3. High energy densities in laboratories

3.1 Main lines of research

The objective of experiments in macroscopic high-energy-density physics consists in the generation of extreme substance parameters whose values are on the verge of modern experimental capabilities. Even now plasma states with peak pressures of hundreds–thousands of megabars, temperatures of up to 10^9 K, and energy densities of 10^9 J cm^{-3}, the latter being comparable to the energy density of the nuclear substance, have come to be subjects of laboratory investigations [3, 4, 22, 29, 64, 65]. According to the notions elaborated to date [23 – 25, 28], to implement a controlled thermonuclear reaction with inertial plasma confinement requires delivering an energy of several megajoules to a spherical target in 10^{-9} s to produce at its center a deuterium–tritium plasma with extremely high parameters: $T \approx (1-2) \times 10^8$ K, $\rho \approx 200$ g cm^{-3}, $p \approx 150-200$ Gbar, which are close to the conditions at the solar center. The corresponding output laser power should exceed the total power of all terrestrial electric power plants by several orders of magnitude. Constructed for this purpose are the National Ignition Facility (NIF) in the USA [3, 4, 66] and LMJ (from French — Laser Mégajoule) in France [67 – 69], as well as soft X-ray radiation facilities involving a high-current Z-pinch (Zeta, USA) [70 – 72] and heavy-ion relativistic beams [73, 74].

These conditions, which are required for the ignition of a controlled thermonuclear reaction, are quite exotic by terrestrial standards, but are quite typical for the great bulk of the Universe's matter compressed by gravitational forces in the interior of stars and other astrophysical objects. In this case there arise several absorbing problems in the physics of high energy densities, with progress in this and allied fields of knowledge depending on their solution [5].

Of fundamental significance is the study of the equation of state of matter and plasma composition in a broad region of the phase diagram, including the conditions inherent in giant planets, exoplanets, dwarfs, giants, and neutron stars, and the determination of quasiclassicality bounds (the Thomas–Fermi model [1, 19]) in thermodynamics. Of considerable interest are the properties of degenerate compressed plasmas and their thermodynamics, equilibrium, kinetic, and trans-

port properties in the conditions of strong nonideality and in the presence of intense magnetic fields, as well as the properties of a quark–gluon plasma and the existence and properties of its hypothetical phase transition.

The intriguing question of a phase transition of the first order in a strongly nonideal plasma has remained open for almost 80 years (see the first data on the observation of this transition in deuterium [54]).

The more distant future will see the studies of the conditions for pycnonuclear reactions ('cold' fusion) and the conditions for strong Coulomb screening which speeds up thermonuclear reactions in the interior of massive stars, as well as the production of relativistic degenerate matter with the Fermi energy $E_F > m_e c^2$ and investigations of its equation of state.

The methods of laboratory energy cumulation that are under development will make it possible to obtain relativistic jets and intense collisional, collisionless, and magnetohydrodynamic shock waves, much like those observed in astrophysical objects [5, 9].

Under discussion are works covering the production of radiation-dominated hot plasmas similar to those existing under the conditions of black holes and accretion disks of neutron stars, as well as the stability of these regimes (experiments involving nuclear explosions [29, 64, 65], lasers [9, 26, 27], and Z-pinches [16, 70 – 72]). Interesting suggestions have been put forward concerning the generation of radiatively collapsing magnetohydrodynamic and collisionless shocks, fast particles, relativistic jets, and their focusing [5, 9, 26, 27].

The high energy density techniques under development open up good possibilities of generating ultrastrong magnetic fields ($B > 1$GG) and investigating their effect on the physical properties of matter. Even now the fields obtained in laser-produced plasmas range into the hundreds of megagausses [75].

Ultrahigh laser power levels may bring closer the prerequisites for the observation of relativistic gravitational effects.

The list may be easily lengthened and is perhaps limited only by our imagination. At the present time, it is hard to tell, even to within tens of years, which of these fascinating problems of high energy density physics will be solved, if at all, at the existing and projected laboratory facilities. However, according to the favorite advice of Academician P L Kapitza, "when going fishing there is a good reason to take the rod with the largest fish hook in the hope of catching the largest fish."

3.2 Generators of high energy densities

The spectrum of experimental facilities for generating high energy densities in macroscopic volumes of matter is highly diversified. It includes diamond anvils for static material compression, gunpowder and light-gas throwing devices — 'guns', explosive generators of intense shock waves, electroexplosion devices, magnetic cumulation generators, lasers, high-current generators of high-power electric current pulses, charged-particle accelerators, and all possible combinations of these devices.

The parameters of the highest-power facilities of different types (lasers, pulsed electrotechnical units, Z-pinches, and particle accelerators), which now are in operation or under construction, are collated in Table 2 [5]. Developed for carrying out plasma research in the interests of defense and

Table 2. Facilities for generating high energy densities [5].

	Laser facilities			*Z*-pinch facilities					
	NIF	LMJ	PW laser	'Sandia'		C-300		Angara V	
				current	XR*	current	XR*	current	XR*
Energy per particle	3.6 eV	3.6 eV	1.5 eV	20 MA	50 – 250 eV	1.5 – 4 MA	70 eV	25 MA	100 eV
Pulse duration	1 – 20 ns	$\sim$ 10 ns	0.5 ps	100 ns (rise time)	5 – 15 ns	80 ns	12 ns	90 ns	6 ns
Spot size	0.3 mm	0.3 mm	5 μm	—	1 mm (cylinder)	—	2 mm	—	2 mm
Pulse energy	1.8 MJ	2 MJ	0.5 – 5 kJ	16 MJ	1.8 MJ	400 kJ	50 kJ	600 kJ	120 kJ
Intensity, W cm^{-2}	2×10^{15}	$\sim 10^{15}$	10^{22}	—	10^{14}	—	$(2-3) \times 10^{12}$	—	$(6-10) \times 10^{12}$
	Accelerators								
	SLAC**		LHC	SIS-18		SiS-100		TSD***	
				Today	Design				
Energy per particle	50 GeV		7 TeV	1 GeV	1 GeV	4 GeV		700 MeV	
Pulse duration, ns	5		0.25	200	50	20		100	
Spot size, mm	3		16	1	1	1		1	
Pulse energy	150 J		334 MJ	$\sim$ 1 kJ	30 kJ	300 kJ		100 kJ	
Intensity, W cm^{-2}	10^{20}		10^{19}	5×10^{11}	6×10^{13}	10^{15}		10^{14}	

* XR — X-ray radiation.
** SLAC — Linear electron accelerator (USA).
*** TSD (terawatt storage device) — accelerating-storage complex at the Institute for Theoretical and Experimental Physics (ITEP).

high-energy physics, they are presently advantageously employed for research in the basic physics of high-energy-density plasmas. The highest-power laser facilities under construction — NIF [13, 66] and the LMJ system [67–69] — will deliver an energy of 1.8–2 MJ in 192 beams in the fundamental harmonic and afford the conditions for the thermonuclear ignition of microtargets. These facilities will make it possible to carry out experiments with shock waves in the gigabar pressure range, thereby advancing to the domain of a quasiclassical description of matter [19], and to study plasma flows under the conditions of developed radiation effects.

In operation in the Russian Federation Nuclear Center 'All-Russia Research Institute of Experimental Physics' (VNIIEF in *Russ. abbr.*)) in the town of Sarov is the Iskra-5 laser facility [78] with an energy of 30 kJ and a pulse duration of 0.3 ns, which is intended for controlled thermonuclear fusion and laser-plasma physics research. The next stage — the Iskra-6 facility — will be 10 times higher in power.

Future progress in this area involves the passage from the petawatt laser power level to the zettawatt one ($\sim 10^{21}$ W). These extremely high power levels can be reached both by shortening the laser pulse duration to an order of attosecond ($\sim 10^{-18}$ s) and by raising the energies of the laser beams (increasing the diameters and number of laser beams in femtosecond facilities). The feasibility of generating an isolated single-cycle 130-attosecond long pulse has recently been demonstrated [79].

Among the multitude of interesting physical experiments with such systems we mention the study of the interaction of ultrashort laser pulses with clusters [80], when their multiple nonequilibrium ionization knocks out electrons from a cluster and stimulates a 'Coulomb explosion' with the production of kiloelectron-volt ions and laser-induced shock waves, and even initiates thermonuclear reactions.

The shortest femto- and attosecond laser pulses are comparable to an oscillation period of light in duration and are a tool for extremely fast action on a substance. The parameters of laser facilities in operation and under construction are given in Fig. 3.

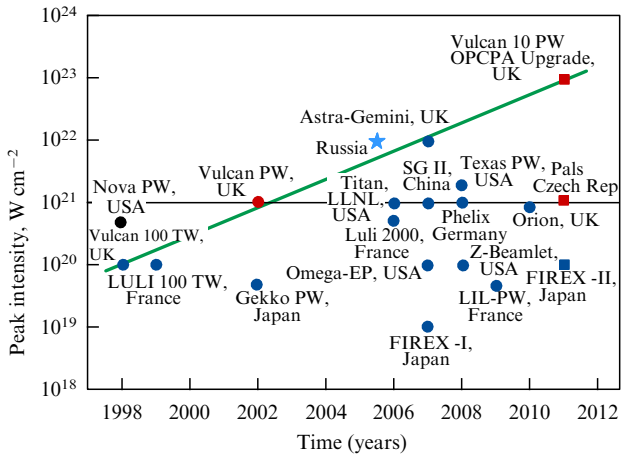

Figure 3. Development of world's petawatt laser facilities (http://www.clrc.ac.uk). Blue circles (see the electronic version of the paper) indicate the presently funded laser facilities, and the blue squares those projected for funding. Red signs correspond to single-beam laser facilities, and the blue ones to ultrahigh-intensity laser facilities with additional capabilities. The black dot stands for the petawatt laser system which operated at the Lawrence Livermore Laboratory. The bold line shows the development trend of the Rutherford Appleton Laboratory (Great Britain). The star denotes the laser facility (VNIIEF + Institute of Applied Physics, RAS) commissioned in late 2006.

3.3 Static and shock-wave techniques

Substantial progress in the area of static pressures was made in the early 1980s with the advent of the experimental technique of diamond anvils [21, 41]. In these facilities, two diamonds cut in a special way compress thin (10–100 μm) plane layers of the substance under investigation to the highest attainable pressures of the megabar range, their upper limit being determined by the diamond ultimate strength of 0.5–1 Mbar. In a number of experiments, the compressed substance was heated by laser radiation (Fig. 4) [81, 82] or the material compressed in diamond anvils was the target for its subsequent compression by laser-driven shock waves [83]. Experiments of this kind have yielded a wealth of useful information about the mechanical properties, thermodynamics, and phase transformations in geophysical objects in the parameter range of $p \approx 0.1-3.5$ Mbar, $T \approx 10^3 - 6 \times 10^3$ K, which is extreme for terrestrial conditions.

Further advancement towards higher energy densities is concerned with the passage to dynamic methods of investigation ([2–4, 12, 22, 29, 32, 33, 35, 36, 42, 64, 65, 84]), which rely on pulsed energy cumulation in the substance under investigation by means of intense shock waves or by means of electromagnetic or corpuscular radiation of a different nature. The plasma temperatures and pressures occurring in this case are far greater than the ultimate thermal strength of the structural materials of the facilities, resulting in limitations on the characteristic plasma lifetime by $10^{-10}-10^{-5}$ s in dynamic experiments, which is governed by the target expansion dynamics. In the dynamic approach there are no fundamental limitations on the magnitudes of the maximum energy density and pressure: they are limited only by the power of the energy source — the so-called driver.

Shock-wave techniques play the leading role in modern high-energy-density physics, making it possible to produce maximum pressures in the megabar and gigabar ranges for many chemical elements and compounds. The peak dynamic pressure attained to date is six orders of magnitude higher than the pressures produced during the impact of a bullet and three orders of magnitude higher than the pressure at the center of the Earth, and it turns out to be close [29, 64, 65] to the pressure in the central layers of the Sun and the targets for inertially confined fusion (ICF).

Not only do shock waves compress a substance, but they also heat it to high temperatures, which is of particular importance for the production of plasma — the ionized state

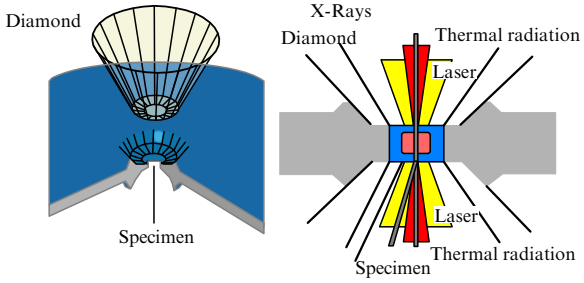

Figure 4. Schematic of a static experiment on the compression of a substance in diamond anvils involving laser heating [82].

of matter. A number of dynamic techniques are presently employed in experimental studies of strongly nonideal plasmas [2 – 4, 33, 35, 36, 56, 84, 85]. They enable producing, behind the shock front, states of nonideal degenerate (the Fermi statistics) and classical (the Boltzmann statistics) plasmas compressed to peak pressures of ~ 4 Gbar and heated to temperatures of order 10^7 K [29, 64, 65], i.e., attaining conditions close to those wherein the energy and pressure of equilibrium radiation begin to play a significant part in the total thermodynamics and dynamics of these high-energy states. These conditions are quite typical of stellar objects at different stages of their evolution.

Multiple shock compression (approximating isentropic one) was used successfully for the experimental study of pressure-induced plasma ionization [11, 12, 22, 54] and substance dielectrization [34] at megabar pressures. Quasiadiabatic compression was also realized in the highly symmetric cylindrical explosive compression of hydrogen and rare gases [11, 22, 54, 56]. Special mention should be made of experiments involving 'soft' adiabatic plasma compression by megagauss magnetic fields [86, 87].

In another limiting case, when obtaining a high-temperature plasma is required, it is expedient to carry out the shock-wave compression of lower (in comparison with solid) density targets, i.e., targets of porous metals [2, 32, 33, 35, 36, 42, 88] or aerogels [89]. This makes it possible to sharply strengthen the irreversibility effects of shock compression and thereby increase the entropy and temperature of the compressed state.

Investigation of the plasma states intermediate between a solid and a gas is made possible by the isentropic expansion technique. This technique involves the generation of plasma in the adiabatic expansion of a condensed substance precompressed and irreversibly preheated at the front of an intense shock wave [2 – 4, 22]. It was precisely this technique that was first employed for the experimental investigation of the high-temperature portions of the boiling curves, the transcritical states, and the metal–insulator transition domains for a large number of metals (for more details, see Refs [2 – 4, 90]).

We see that dynamic techniques in their different combinations permit realizing in experiment and investigating a broad spectrum of plasma states with a variety of strong interparticle interactions.

At present, use is made of a substantial number of energy sources for the dynamic cumulation of high energy density in dense media.

Today, the technique of intense shock waves generated by impacts of metal liners (strikers), which are accelerated to velocities of several kilometers per second, on a target of the substance under investigation is the main source of the physical information about plasma behavior at pressures of up to 10 – 15 Mbar. Here we shall not describe at length the liner explosive acceleration technique and the means of diagnostics — they are the concern of comprehensive reviews and monographs [2 – 4, 9, 11, 12, 22, 29, 32, 33, 35, 36, 91, 92]. We only note that in shock-wave experiments of this kind it is possible to carry out sufficiently ample measurements of the plasma physical properties.

Specific plasma energy densities, which were record-high for terrestrial conditions, were obtained in the near-source zone of a nuclear explosion [29, 33, 64, 65, 91 – 93] (Fig. 5). The world-record plasma pressure reached in terrestrial quasilaboratory conditions amounts to 4×10^9 atm [64], which is close to the pressure in internal layers of the Sun.

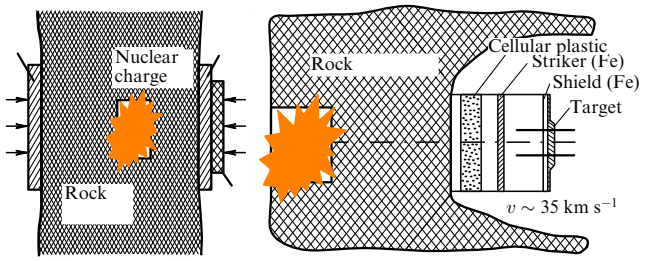

Figure 5. Schematic of experiments on the generation of intense shock waves in the near-source zone of a nuclear explosion [29, 65, 92, 93].

The plasma under these conditions ($W \approx 10^9$ J cm^{-3}, $n_e \approx 4 \times 10^{24}$ cm^{-3}, $T \approx 8 \times 10^6$ K) is nondegenerate, $n\lambda^3 \approx 0.07$, twelve-fold ionized, and its nonideality parameter is rather small, $\Gamma \approx 0.1$, which serves as an experimental illustration of the thesis of Section 2 about simplification of the physical plasma properties in the limit of ultrahigh energy density.

Obtained in nuclear explosions [29, 32, 33, 64, 65, 91, 92] were pressures in the multimegabar range, close to the characteristic 'physical' pressure $p \sim e^2/a_B^4 \sim 300$ Mbar, and temperatures $T \gg \mathrm{Ry} \sim 10^5$ K. Beginning from these latter values, the Thomas–Fermi model can be applied [1, 19], which implies a simplified quantum-statistical description of a strongly compressed substance and the 'self-similarity' of its physical properties with respect to the nuclear charge.

The question concerning the limits of validity of the quasiclassical model is still, to a large extent, an open question and the behavior of substances in the $p > 300$ Mbar region turns out to be more diversified than previously assumed on the basis of simplified notions [19]. Experimental verification of the predictions of the quasiclassical shell model is one of the most interesting problems of ultrahigh-pressure physics; solving this problem would supposedly call for new experimental techniques relying on intense directed energy fluxes (see Sections 3.4, 4, and 5.1).

The reader interested in ultrahigh-pressure problems is referred to Refs [2, 22, 29, 56, 64, 65, 91, 92].

3.4 Electrodynamic methods

High-current ($10^5 - 10^7$ A) pulsed energy devices are employed to produce high energy density plasmas in various kinds of experimental facilities. Electric energy may effect the direct pulsed Joulean heating (electroexplosion) of conductors or the magnetohydrodynamic compression and heating of plasma objects. The stored energy may be used to produce intense bursts of soft X-ray radiation (with a radiation temperature of 200 – 300 eV) with the subsequent generation of intense shock or thermal radiative waves by this radiation, or for the electrodynamic generation of shock waves, as well as for the electrodynamic acceleration of metallic liners. The energy capabilities of electrodynamic devices of this kind are, as a rule, several orders of magnitude higher than those of lasers (with the exception of NIF and LMJ), making it possible to conduct experiments with thicker targets and thereby to improve the accuracy of measurements and reduce the time-resolution requirements ($10^{-8} - 10^{-7}$ s) on the means of diagnostics.

The electroexplosion of conductors and metal foils caused by the passage of a pulsed current of 50 – 200 kA is the

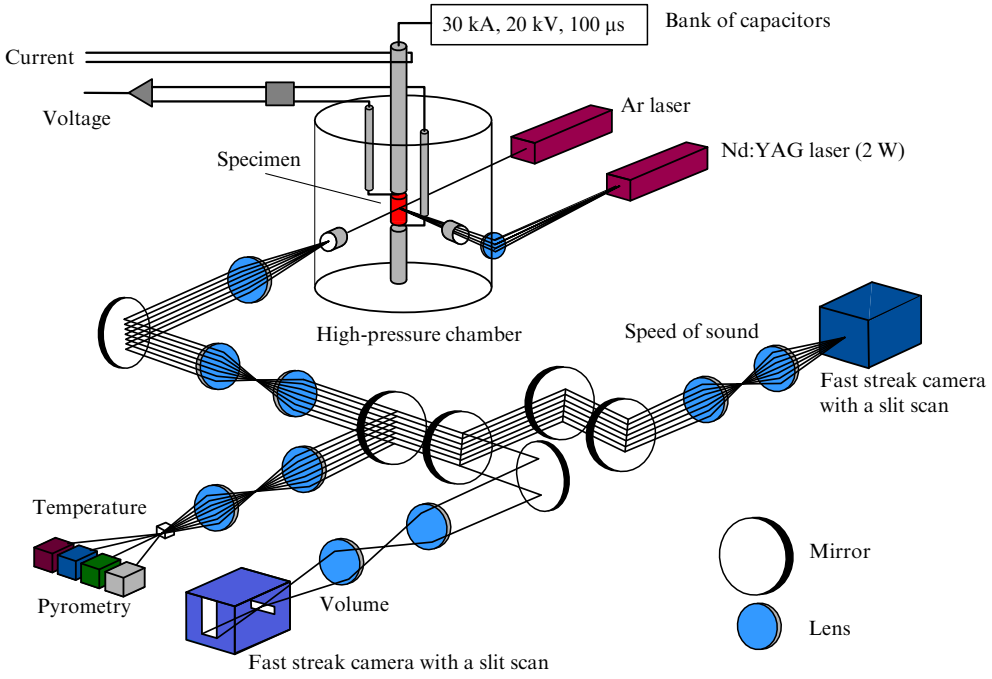

Figure 6. Schematic representation of exploding-wire experiment [94].

traditional line of research into the thermophysical properties of refractory materials in the domain of the condensed state [94] for characteristic energy densities of order 10 kJ cm^{-3} (Fig. 6). This range was recently extended to 20 – 30 kJ cm^{-3} with the attainment of strongly supercritical metal states, which permits, in accordance with the suggestion of Landau and Zel'dovich [95], studying the 'metal–insulator' transition during the continuous supercritical expansion of metal plasmas.

To date, the highest plasma parameters have been obtained in *Z*-pinches of the terawatt power range, in which the electric energy of capacitors, after the corresponding sharpenings, accomplishes electrodynamic plasma acceleration followed by the focusing of its kinetic energy on the cylinder axis [96, 97]. In this way, a 10-ns long burst of soft (150 – 200 eV) X-ray radiation with an energy of $E \approx 1.8$ MJ and a power of 230 TW was produced on the *Z*-pinch facility in the Sandia Laboratory (USA) [70 – 72]. In these experiments, a cylindrical plasma shell was produced by the electric explosion of several hundred thin (6 – 50 μm) tungsten wires through which a 20-MA current pulse with a rise time of about 100 ns was passed. Tungsten plasma with an ion number density of order 10^{20} cm^{-3} and a degree of ionization higher than 50 was obtained under the axial collapse. The second interesting application of this facility involves the electrodynamic generation of intense shock waves [15].

In experiments at the high-current Angara facility [16], a pulsed current of $j \approx 4$ MA accelerated a xenon plasma liner to a velocity of approximately 500 km s^{-1}. The highly symmetrical impact of this liner on the surface of a highly porous cylindrical target generated a thermal radiative wave in it, which emitted soft X-ray radiation with a temperature of about 100 eV. This high-intensity X-ray radiation from the cylindrical cavity was utilized for the highly symmetrical generation of plane shock waves with a pressure amplitude of about 5 Mbar for exciting thermal radiative waves with a

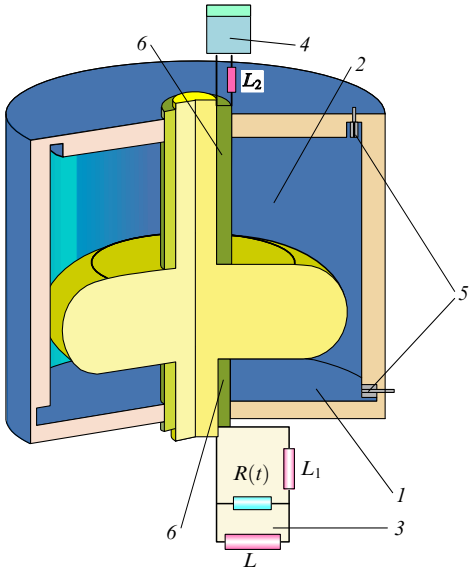

Figure 7. Schematic of the MAGO plasma generator [101]: *1*, *2* — plasma chamber; *3*, *4* — power sources, explosive magnetic generators; *5* — sensors, and *6* — insulators.

propagation velocity of 100 km s^{-1}, as well as for accelerating metallic liners to velocities of 10 – 12 km s^{-1}.

Interesting plasma parameters were reached in *Z*-pinches with an initially gaseous shell [96, 97] and in the *X*-pinch geometry obtained by crossing two current-carrying wires [98, 99].

In the operation of modern high-current pinches, in the course of production of high energy densities there occur developed magnetohydrodynamic flows wherein the crucial role is played by radiation [100], which is of significance in its own right in radiative gas-dynamic simulations of astrophysical objects.

In the Magnetic Compression (MAGO in *Russ. abbr.*) Project (Fig. 7) [101], a pulsed current of 7 MA delivered by an explosive magnetic generator [102, 103] compresses and heats a preliminarily prepared magnetized plasma to bring it to a state close to the thermonuclear conditions: $\rho \approx 20$ g cm^{-3}, $T \approx 3-4$ keV, which furnishes a DT-reaction neutron yield of $(3-5)\times 10^{13}$. In this case, an energy density $W \approx 10^7$ J cm^{-3} is realized in the plasma-compressing metallic liner.

The Baikal facility [104, 105] projected in Russia should become a source of soft X-ray radiation with an output energy $E \approx 10$ MJ intended for experiments with indirect-driven thermonuclear targets and other problems of high energy density physics. By employing the X-1 facility, which feeds two pinch units, each generating 7 MJ of soft X-ray radiation with a power of 1000 TW, it is planned to further develop the success achieved at the Z facility (Sandia Lab., USA).

The use of chemical explosives for generating intense pulsed currents and magnetic fields [86] relies on the explosive compression of the initial magnetic flux by conducting metallic liners [86, 87, 102] accelerated to velocities of several kilometers per second by the detonation products of condensed explosives. This is precisely the way it has been possible to reach the values of electric current of ~ 300 MA and magnetic induction of ~ 29 MG, which are the record values achieved under terrestrial conditions [103]. In the latter case, the magnetic field energy density was equal to 3×10^6 J cm^{-3}, making it possible to carry out interesting physical experiments in megagauss magnetic fields: the quasi-isentropic compression of substances [86, 87], the study of magnetoresistance, magnetooptical effects, the de Haas–Shubnikov effect, and many other phenomena revealing themselves at high energy densities [106].

4. High-power lasers in high energy density physics

The rapid progress of laser technology has brought existing and projected laser complexes into the petawatt–zettawatt power range (see Table 2 and Figs 3 and 8), making it possible to span a wide range of power densities up to the highest values achievable today: $q \approx 10^{22}-10^{23}$ W cm^{-2} [27, 45, 46, 107, 108], which will undoubtedly rise with time. The action of these enormous intensities on targets leads to diverse new physical effects in hot plasmas [27, 63, 109], such as multi-photon ionization, self-focusing and filamentation of a different nature, the generation of superintense electric and magnetic fields, electron and ion acceleration to relativistic velocities, nuclear reactions caused by these fast particles, relativistic plasma 'transparentization', nonlinear modulation and multiple harmonic generation, ponderomotive effects in hydrodynamics, and many other effects which are the subject of vigorous research today (see reviews [26, 27] and references cited therein).

Some of these effects will be briefly considered in this section.

The further growth of laser radiation power density will be accompanied by qualitatively new phenomena [5], like spontaneous electron–positron pair production (the 'boiling of a vacuum' and its loss of transparency [5, 14, 23–27, 55–61, 63, 110], the emergence of microscopic quantities of relativistic matter, the generation of relativistic shock waves and plasma streams, solitons, jets, and γ-ray bursts similar to the astrophysical ones, and — in perspective — the realization

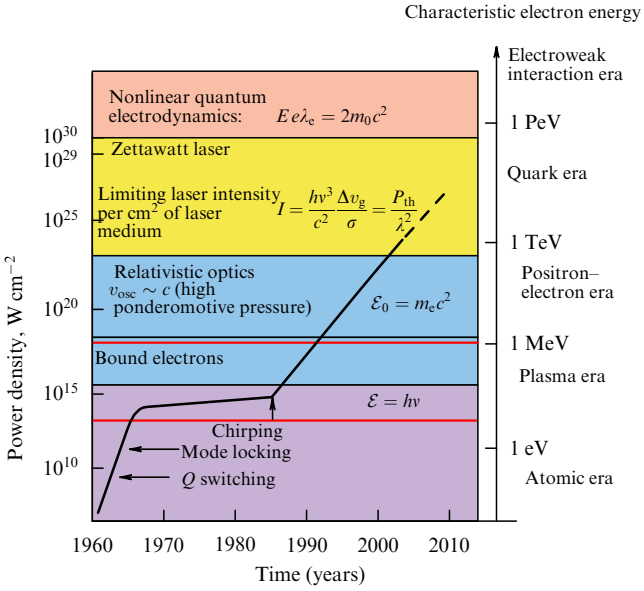

Figure 8. Growth of laser radiation intensity with time [5, 27]. The rapid rise in radiation intensity in the 1960s resulted in the discovery of numerous nonlinear effects induced by bound electrons (characteristic energies of ~ 1 eV). The intensity attained to date permits studying the processes at relativistic electron energies ($\mathcal{E}_0 \sim m_e c^2 \sim 0.5$ MeV).

of conditions where quantum gravitation shows up [111–113]. This new level of an action intensity may see the advent of new schemes of controlled thermonuclear fusion, nuclear reactions, and new ways of producing short-lived isotopes, as well as extraordinary schemes of high-efficiency compact accelerators.

Figure 8 shows the progress in increasing the irradiation intensity and the possibilities that open up for studying the processes in high-energy-density physics [5, 27].

The present-day renaissance in laser physics is related to the invention of the chirped optical pulse technique (see Fig. 8) in 1985 [114–118], which opened up the way for multiterawatt, petawatt, and even exawatt laser systems to raise the peak intensities on a target to $q \approx 10^{22}$ W cm^{-2}, with the theoretical limit equal to 3×10^{23} W cm^{-2}. In this technique [114–118], an initially short laser pulse is stretched in time, following which this lower-intensity pulse is amplified in a laser-active medium and is then compressed.

The chirp technique has made it possible to raise the initial intensity of laser radiation by 5–6 orders of magnitude and to radically lower the cost and dimensions of lasers which have become desktop devices affordable even for university laboratories. Furthermore, these lasers combine well with big facilities for controlled laser fusion ('fast' ignition) and charged-particle accelerators (see Section 5.1, Fig. 11b), providing also the possibility of recording nonlinear quantum-electrodynamic effects like pair production in a vacuum [61, 63, 119] and of generating intense optical radiation for studying photon–photon collisions [120].

The advent of this high-power laser technology has enabled a substantial advancement along the intensity scale and has made it possible in laboratory research to move from studies of atomic and solid-state processes to studies of hot plasmas, laser nuclear physics, high-energy physics, relativistic physics, and, in the future, perhaps, cosmology beyond the Standard Model [7, 27, 45, 46].

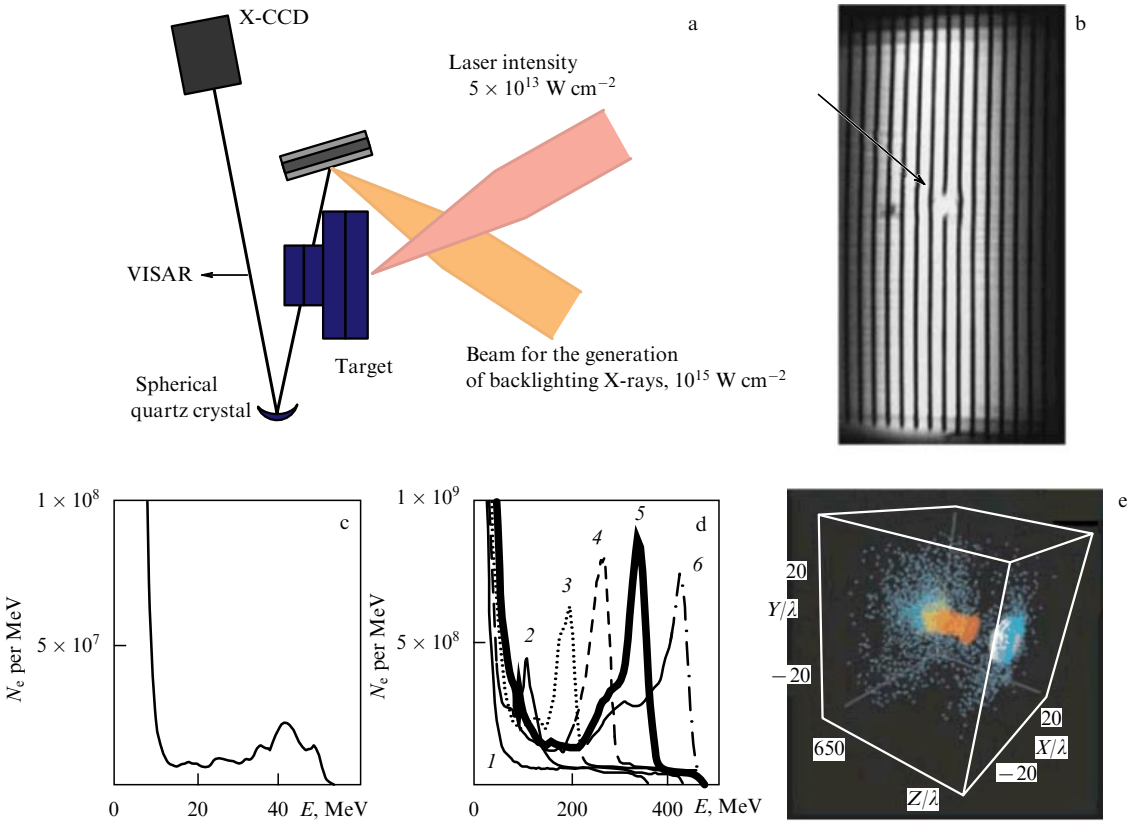

Figure 9. Experiments (a) with laser-driven shock waves [121] involving the measurement (b) of the density of shock-compressed plasma from the absorption of 5-keV X-ray radiation. X-CCD is an X-ray charge-coupled device, and VISAR is a system for improving image's clarity. Energy spectrum of electrons [26, 122] accelerated by laser radiation with pulse energy and duration of (c) 20 mJ, 6.6 fs and (d) 12 J, 33 fs; temporal evolution of the spectrum: *1* — $ct/\lambda = 350$, *2* — $ct/\lambda = 450$, *3* — $ct/\lambda = 550$, *4* — $ct/\lambda = 650$, *5* — $ct/\lambda = 750$, and *6* — $ct/\lambda = 850$. (e) Propagation of a laser pulse (12 J, 33 fs, $z/\lambda = 690$) through a plasma with a concentration of 10^{19} cm^{-3}: three-dimensional picture of nonthermal electron energy distribution for $q \sim 10^{19}$ W cm^{-2}. Shown are above-10 MeV electrons; in this case, electrons that differ in energy by more than 10 keV are indicated by different colors.

The action of high-power laser radiation leads to new strongly nonlinear physical phenomena in relativistic plasmas with pressures ranging into the gigabars, with electric field strengths of several teravolts per centimeter, and gigagauss magnetic field [26, 27] (see Fig. 8).

In addition to the well-known effects of self-focusing, stimulated scattering, and laser pulse front steeping there emerge new challenging effects: light filamentation, relativistic and ponderomotive effects in hydrodynamics, and fully developed generation of nonthermal gigaelectron-volt electrons and multimegaelectron-volt ions in laser plasmas, which result in nuclear reactions [5, 26, 27]. Here, we are dealing with extremely short — femtosecond — durations of a laser pulse, during which the electromagnetic wave undergoes only a few oscillations.

Let us start to ascend the curve in Fig. 8. Beginning with $q > 10^{14}$ W cm^{-2} (for $\lambda = 1$ μm), the pressure amplitudes of laser-driven shock waves pass into the megabar range [14, 23, 24, 26, 27] in accordance with the scaling law

$$p\,[\mathrm{TPa}] = 0.87\big(q\,[\mathrm{W\ cm^{-2}}]\big)^{2/3}\ \big(\lambda\,[\mu\mathrm{m}]\big)^{-2/3},$$

where λ is the wavelength of laser radiation in micrometers.

Beginning with $q > 3.4 \times 10^{18}$ W cm^{-2}, the electric field strength $E = \sqrt{4\pi q/c}$ in the laser wave is comparable to the strength of the electric field of the nucleus, $E_a = e/a_B^2 \approx 5 \times 10^9$ V cm^{-1}, in the first Bohr orbit of a hydrogen atom. To ionize the energy level U_i requires a laser intensity

$$q = \frac{4 \times 10^9\, U_i^4}{Z^2}\ [\mathrm{W\ cm^{-2}}],$$

where Z is the charge number.

Under these conditions, laser radiation ionizes the medium which turns into a heated plasma. Interesting experiments are being conducted in this parameter range on the generation of intense shock waves by laser radiation [14, 121] (Figs 9a and 9b) and on the production of fast charged particles in laser plasmas [26, 57–59, 63, 122] (Figs 9c–9e). Beginning with roughly the same laser intensities $q > 10^{17}$ W cm^{-2}, nonthermal electrons and ions in the ultramegaelectron-volt range are generated in the absorption region [57–59, 122]. Beginning with $q \sim 10^{18}$ W cm^{-2}, the ponderomotive light pressure turns out comparable to the hydrodynamic plasma pressure [5, 23, 24, 26, 27].

Relativistic effects become significant when the kinetic energy of an electron accelerated in a laser wave field is of the order of $m_e c^2$ (where m_e is the electron rest mass), which leads to the condition

$$q_{pe}\,\lambda^2 \sim 1.37 \times 10^{18}\ \mathrm{W\ \mu m^2\ cm^{-2}},$$

and when $\lambda = 1$ μm it appears that $q_{pe} \sim 10^{18}$ W cm^{-2}.

Therefore, for the first time it has become possible to obtain in terrestrial conditions a microscopic quantity of a

substance with relativistic energies [26, 27] for the effective electron mass of order $100\,m_e$.

Proton motion will become relativistic at intensities

$$q_{pp} = \left(\frac{M_p}{m_e}\right)^2 q_{pe} \sim 5 \times 10^{24}\ \mathrm{W\,cm^{-2}}\,,$$

which will hopefully be realized soon in experiments.

The passage to 'relativistic' intensities of laser radiation has already brought [27] several interesting physical results [107]. The case in point is the generation of X-ray [123] and gamma-ray [124] radiation, relativistic self-focusing [125], higher harmonic generation [126, 127], the acceleration of electrons [26, 63, 128], protons [129], and ions [57 – 59, 130], neutron [131] and positron [132] production, appearance of electron vortices and solitons [26, 27, 133], ultramegagauss magnetic field generation [134], and manifestations of quantum electrodynamic effects [61, 63, 135].

Under high-intensity irradiation, relativistic plasma transparentization occurs [5, 26, 27], which is related to the relativistic growth in electron mass and the corresponding lowering of the critical plasma frequency $\omega_p = \sqrt{4\pi e^2 n_e/\gamma m}$ (where γ is the relativistic Lorentz factor), to the plasma density modification by ponderomotive forces, and to the frequency transformation of the laser pulse itself [132].

Along with the relativistic plasma transparentization effect, of considerable interest is the effect of relativistic self-focusing of laser radiation [27] caused by plasma permittivity variation due to the relativistic growth in electron mass in the transverse direction relative to the beam propagation direction and the spatial plasma density redistribution under the action of ponderomotive forces. The critical power W_c for self-focusing was derived by Norreys et al. [124] and Sarkisov et al. [125]:

$$W_{cr} = \frac{m_e c^5 \omega^2}{e^2 \omega_{pe}^2} \sim 17\left(\frac{\omega}{\omega_{pe}}\right)^2\ [\mathrm{GW}]\,.$$

Experiments staged to observe this effect were reported in Refs [126, 128]. Particle-in-cell simulations [26] reproduce the multiray structure of a laser pulse, occurring due to filamentation instability and the buildup of transverse beam nonuniformity which resembles the self-focusing phenomenon. The self-focusing and filamentation of laser radiation in plasma result in the formation of electron vortices [129], high-intensity compensative currents, and the generation of strong magnetic fields. Measurements of Refs [131, 136, 137] for a laser radiation intensity of 9×10^{19} W cm^{-2} yielded a magnetic field induction of 340 MG, which is an order of magnitude higher than the record inductions obtained employing explosive magnetic generators [86, 87, 102, 103].

Similar interesting effects of a relativistic nature [24, 26] are related to strongly nonlinear plasma waves which form vacuum channels and 'bubbles' in the plasma, produce plasma lenses for charged particles, and give rise to intense electromagnetic radiation in the frequency range from terahertz oscillations to X-rays, as well as excite collisionless shock waves [27].

The propagation of two collinear laser beams of relativistic intensity through a plasma [109] leads to the generation of intense electromagnetic wake waves. These wake waves enable accelerating electrons under electric field gradients up to 100 MV cm^{-1}, which are thousands of times greater than ordinary acceleration gradients (~ 5 kV cm^{-1}). Gigantic longitudinal electric fields are generated in this case [63]: for a laser intensity $q \sim 10^{18}$ W cm^{-2}, the electric field strength is ~ 2 TV m^{-1}, for $q \sim 10^{23}$ W cm^{-2} it amounts to ~ 0.1 PV m^{-1}. These acceleration rates imply that the laser version of the 50-GeV SLAC particle accelerator would be only 100 μm long [63]. Successful experiments have been carried out recently on the laser-driven acceleration of electrons to energies of 10 – 170 MeV at laser radiation intensities of $10^{18} - 10^{19}$ W cm^{-2} [138, 139]. There are grounds to believe that the advent of multipetawatt and exawatt lasers in the future would lead to the implementation of acceleration rates of the order of several teravolts per centimeter for a total electron kinetic energy ranging into the gigaelectron-volts.

Quantum optical effects come into play at $q \approx 1.4 \times 10^{26}$ W cm^{-2} [63], the electron kinetic energy being equal to ~ 50 TeV in this case. For $q \sim 10^{21}$ W cm^{-2}, the light pressure is equal to ~ 300 Gbar, which is close to the pressure at the center of the Sun and is much higher than the pressure in the near-source zone of a nuclear explosion [29, 64, 65, 92].

High-intensity lasers make it possible to achieve superstrong acceleration $a_e \approx 10^{30} g$, which is close to the accelerations in the vicinity of the Schwarzschild radius of a black hole [8, 140] (see Section 6.2). This open up the fundamental possibility to model the conditions in the neighborhood of black holes and wormholes, and thereby verify the predictions of the general theory of relativity.

In particular, for $q \sim 10^{26}$ W cm^{-2} the electron acceleration amounts to $a_e = 10^{27} g$, which is close to the conditions of the black-hole event horizon [5, 7, 8, 10]. If such acceleration is realized, an opportunity will supposedly open up to study the specific Unruh electromagnetic radiation [111 – 113], which is similar to the Hawking radiation caused by gravitational effects.

At higher laser radiation intensities, $q \sim 3 \times 10^{29}$ W cm^{-2}, there is a good chance to verify the predictions of modern quantum gravity theories [7, 141 – 144] about the change in the space–time dimensionality at short distances r_n. According to Arkani-Hamed et al. [142], the latter quantity is evaluated as $r_n \sim 10^{32/n-17}$ cm, where the dimensionality $n > 4$. In this case, the electron wave function will be reflective of a different law of gravitation for $n \leqslant 3$ at distances of order 10^{-6} cm.

The effects of quantum electrodynamics, polarization, and then of the emergence of quark–gluon plasma become significant at ultrahigh optical radiation intensities $q > 3 \times 10^{29}$ W cm^{-2}.

The problem of spontaneous electron–positron pair production in a vacuum touches upon many interesting effects, like the collisions of heavy ($Z_1 + Z_2 > 135$) nuclei [145], the evaporation of black holes [146], particle production in the Universe [147], and so forth. The characteristic electric field scale [5] for the manifestation of the breakdown effect in quantum electrodynamics is the Schwinger strength

$$E_S = \frac{m^2 c^3}{e\hbar} \approx 10^{16}\ \mathrm{V\,cm^{-1}},$$

which is sufficient to accelerate an electron to relativistic velocities over the Compton wavelength $\lambda_C = 2\pi\hbar/(mc)$ and corresponds to ultrahigh laser radiation intensity

$$q_{QED} = q_{pe}\,\frac{\lambda^2}{\lambda_C^2} \approx 8.1 \times 10^{30}\ \mathrm{W\,cm^{-2}}\,.$$

This intensity threshold for electron–positron pair production is substantially lowered (to 10^{22} W cm^{-2}) in the case of scattering by nuclei [148 – 150]. The composition of two counterpropagating laser beams yields a critical intensity of 10^{26} W cm^{-2} for pair production, which is two orders of magnitude below the limit value for a single beam [151].

The high energy densities delivered to laser plasmas turn out to be sufficient not only for diverse electronic processes, but also for nuclear transformations like activation, fission, fusion, and transmutation of nuclei [63, 152, 153]. The photonuclear fission of uranium and then of thorium was successfully demonstrated in Refs [153 – 156]. Recently, Magill et al. [157] realized (as a result of the (γ, n)-reaction) the laser-induced transmutation of ^{129}I isotope — the main radioactive waste component with a half-life of 15.7 million years — into ^{128}I isotope with a half-life of 25 minutes.

Among the possible applications of laser-induced photonuclear reactions [152] mention should be made of the production of radioactive isotopes for medicine, the transmutation of long-lived isotopes, the determination of nuclear constants, and radioactive material detection for antiterrorist purposes, etc.

Owing to a high efficiency ($\sim 12\%$ [154]) of laser radiation energy transformation into the energy of high-energy protons, the latter may be utilized for the development of pulsed neutron sources whose operation is based on the nuclear reactions (p, xn) and (p, f). In any case, the neutron flux [152] may far exceed the intensity of the flux ($\sim 10^5$ neutrons per joule) produced by the Coulomb explosion of deuterium clusters.

As noted in the foregoing, in the field of high-intensity laser radiation there occurs production of positrons which annihilate with target electrons to emit two photons with an energy of 0.511 MeV. An analysis of the spectra of this radiation yields valuable information about the electronic properties of the target. Therefore, positron sources are presently employed in annihilation positron spectroscopy, in materials science, in positron spectroscopy, in fundamental research, etc. Low-energy positrons find use in electron–positron plasma research, atomic and molecular physics, antihydrogen production, simulations of astrophysical phenomena, and materials science.

Electrons and ions accelerated in laser plasmas may be employed to produce isotopes through a series of (γ, n) and (p, n) nuclear reactions. Such devices are more compact than existing cyclotrons and may be located directly in clinics, being employed, for instance, for positron-emission tomography [74, 158 – 160]. In particular, at the Lawrence Berkeley National Laboratory (USA) a laser-plasma electron accelerator based on a 10-terawatt solid-state laser was employed to produce ^{62}Cu and ^{61}Cu isotopes in the (γ, n) reaction with ^{63}Cu. Considerable recent attention in the USA, Europe, and Japan has been attracted to the idea of constructing laser-plasma accelerators of protons with energies of the order of 200 MeV for different medical applications.

Electron–positron pair production under laser irradiation was reported in Refs [61, 63, 148 – 151, 161], where observations were made of other interesting effects as well, like multiphoton interference and the vacuum polarization. Nonlinear Compton scattering and pair production was evidenced in the course of interaction between laser radiation ($q \approx 5 \times 10^{18}$ W cm^{-2}) and 46.6- and 49.1-GeV electrons accelerated by SLAC accelerators [5].

Tajima [162] proposed employing a high-energy (8 GeV) electron accelerator (Spring-8) and high-power lasers for experiments in quantum electrodynamics and the generation of high-intensity γ-ray radiation for photonuclear reactions. In this case, a study can be made of the interplay between strong and weak interactions. Combining accelerators with lasers may hold much promise for the development of new-generation optical sources, like femtosecond synchrotrons and coherent X-ray radiation sources [5, 163].

The manifestation of qualitatively new physical effects in the advancement along the laser intensity scale (see Fig. 8) is now hard to predict, for we know too little about the structure of matter at ultrahigh energy densities in the immediate spatio–temporal neighborhood of the Big Bang.

5. Relativistic charged particle beams

The highest energy density attainable under terrestrial conditions is generated in relativistic heavy-ion collisions. Accelerators [74] required for this purpose operate in several of the world's laboratories and are well known as the principal experimental tool in nuclear physics, elementary particle physics, quantum chromodynamics, and superdense nuclear matter physics research [7, 45, 46, 164, 165], i.e., in the fields which have always been in the forefront of natural sciences.

Accelerator science and technology have come a long way, from the first 1.2-MeV proton cyclotron invented by E Lawrence in 1932 to the Large Hadron Collider (LHC) with energies of 7 TeV in either of the counter-propagating beams. During this period, the world saw the construction of tens of accelerators of different types, which are giant electrotechnical facilities accumulating cutting-edge engineering ideas and exhibiting a high degree of reliability.

In particular, the Stanford Linear Accelerator, USA, generates a five-picosecond pulse of 10 electrons with a kinetic energy of 50 GeV, which is focused on a 3-μm-sized spot to provide a power density of 10^{20} W cm^{-2}.

The LHC acceleration complex will make attainable a new TeV-energy region, which would supposedly be sufficient for the production of dark matter particles of mass $m_{DM} \sim 10$ GeV – 1 TeV, the Higgs boson, and quark–gluon plasma, and for solving other extremely interesting problems of high-energy physics [47, 166]. Later on, it will be possible to study the processes in the collisions of highly ionized lead ions (Pb^{82+}) with energies of up to 155 GeV per nucleon. The actively operating Relativistic Heavy Ion Collider (RHIC) of the Brookhaven National Laboratory (USA) affords an energy up to 500 GeV per nucleon in the center-of-mass system for colliding gold ions [167]. The new experimental data obtained at this accelerator are discussed in Ref. [168]. In Darmstadt (Germany), a start was made in November 2007 on the construction of a unique antiproton and ion accelerator facility called FAIR (Facility for Antiproton and Ion Research) with an energy of 1.5 – 34 GeV per nucleon for the respective numbers of accelerated U^{92+} ions and antiprotons of $\sim 5 \times 10^{11}$ and 4×10^{13}. The construction cost of each of these major ultrarelativistic hadron accelerator complexes amounts to several billion dollars and is close to the limit of economic capabilities of the world's wealthiest countries and even international communities like the European Union.

For our consideration it is significant that these acceleration experiments are aimed at the production of particle

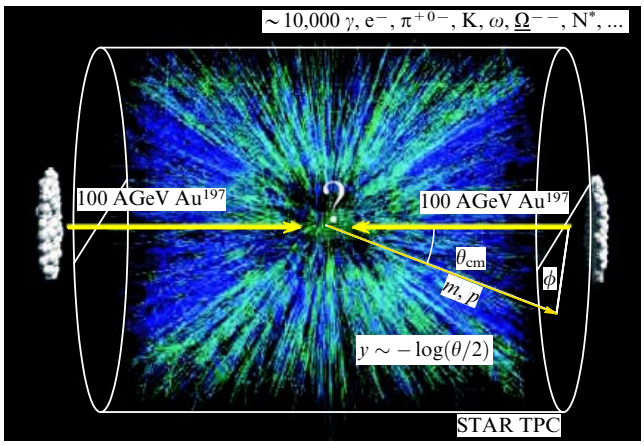

Figure 10. Relativistic hadron collisions — 'burning' of vacuum [169].

beams with ultrarelativistic energies for the investigation of individual hadron collision events (Fig. 10) [169], as well as for macroscopic substance heating [73, 74, 170].

5.1 Production of macroscopic hot plasma volumes

A significant attractive feature of charged particle beams is the bulk nature of their energy release [73]. This distinguishes them from laser radiation: the major portion of energy of radiation with a frequency ω_{laser} is released in a narrow critical zone [14, 23–25] $\omega_{\text{laser}} \approx \omega_{\text{p}} \approx \sqrt{4\pi e^2 n_{\text{e}}/m_{\text{e}}}$ and is then transferred into the target interior through electron thermal conduction [14, 23–25]. The deceleration of charged particles results in the appearance of a layer of isochorically heated plasma, whose subsequent expansion generates a shock wave directed into the target interior or a cylindrical shock wave converging on the beam axis. Modern research in high energy density physics takes advantage of both techniques: isochoric heating and compression by shock waves generated by corpuscular beams.

For corpuscular beam generators use is made of either synchrotrons designed for studies in high-energy physics and nuclear physics [170] or high-current diode systems [171, 172]. In the latter case we are dealing with subnanosecond current pulses of the megaampere range with a kinetic particle energy of 1–20 MeV [50, 51].

In experiments reported in Ref. [173], a relativistic electron beam with a megaelectron-volt energy was employed to excite shock waves in aluminium targets for the purpose of studying the absorption of electrons in dense plasmas and elucidating the effect of intrinsic magnetic fields of a beam on its stopping power in the magnetized plasma (magnetic 'stopping' effect).

Owing to a substantially shorter ion range in comparison with the electron range, ion beams enable obtaining a higher energy density in the plasma. In a series of works [171] performed at the KALIF (Karlsruhe Light Ion Facility) pulsed high-current accelerator, a proton beam with an energy of $E \approx 2$ MeV and a current of $j \approx 400$ kA produced a power density of order 10^{12} W cm^{-2} on the target. This enabled accelerating thin (50–100 μm) strikers to a velocity of 12–14 km s^{-1} and carrying out substantive measurements of the stopping power for fast protons in dense plasmas, recording the thermodynamic parameters and viscosity of shock-compressed plasma, and determining the split-off strength of metals under high strain rates on record. It turned out, for instance, that the split-off strength of metals substantially rises (by 1–2 orders of magnitude) with an increase in the strain rate, to approach its theoretical limit, which is related to the propagation kinetics of dislocations and cracks in the pulsed tension field [171, 174, 175].

Developed for experiments in high-energy physics, relativistic heavy-ion accelerators turned out to be promising candidates (see Table 2) for inertial CTF and experiments on the compression and heating of dense plasmas [73, 74].

The Large Hadron Collider (Fig. 11) generates 2808 0.5-ns long bunches with 1.1×10^{11} protons in each; two successive bunches will be separated by 25 ns, so that the total

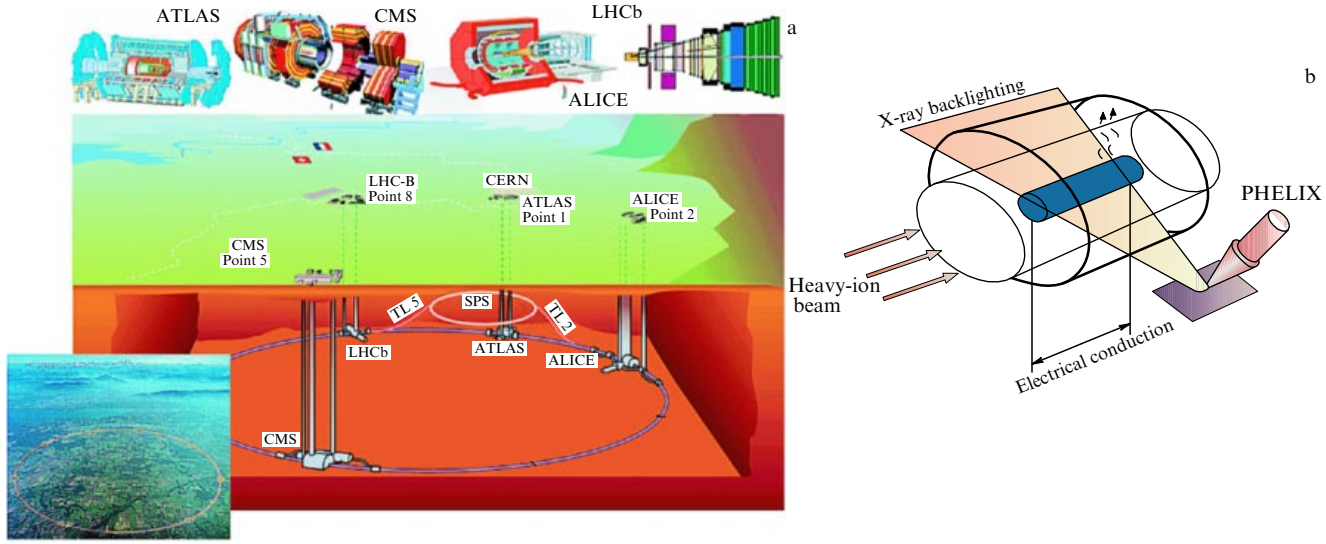

Figure 11. (a) Schematic of the Large Hadron Collider (LHC). The LHC underground tunnel measures about 27 km in diameter. The Super Proton Synchrotron (SPS) serves as a preliminary accelerator. Depicted at the top of the picture are the main detectors: ALICE (A Large Ion Collider Experiment), ATLAS (A Toroidal LHC ApparatuS), CMS (Compact Muon Solenoid), and LHCb (LHC Beauty Experiment). The bottom-left inset presents a general view of the LHC. (b) Schematic of the experiment involving a relativistic heavy-ion beam and the petawatt PHELIX laser [74, 170–180].

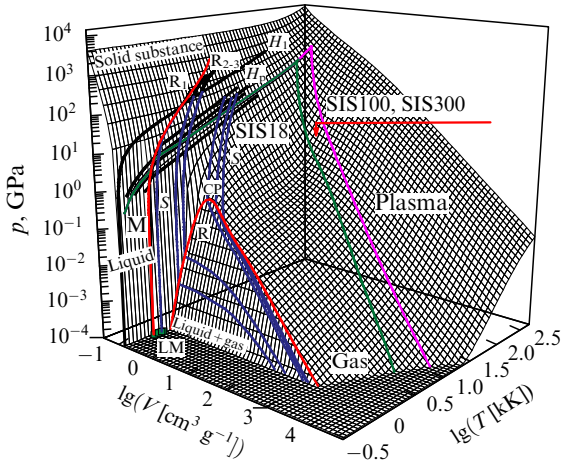

Figure 12. Portions of the phase diagram of zinc attainable with heavy-ion generators [74, 170, 179, 180]: H_1 — the main shock adiabat, H_p — shock adiabats of porous zinc, S — unloading isentropes of shock-compressed zinc, M — melting region, R — evaporation region with a critical point CP, LM — measurements of liquid metal density at atmospheric pressure.

duration of the beam will be about 89 μs, and the total energy will reach $E \approx 350$ MJ — a quantity of energy sufficient for melting 500 kg of copper. The energy density in one beam reaches 10^{10} J cm^{-3}. The characteristic kinetic energy of one relativistic heavy ion is comparable to the kinetic energy of a metal liner accelerated by the explosion products in the explosive throwing system described in Section 3.3.

Heavy-ion beams with a kinetic energy of 3 – 300 MeV per nucleon were employed in experiments on the heating of condensed and porous targets, measurements of the plasma stopping power for ions, and the interaction of charged beams with shock-compressed plasmas produced by mini-explosion shock tubes [74, 176 – 179].

Of special interest is the project to use the SIS heavy-ion accelerator in the Helmholtz center for heavy ion research (GSI-Darmstadt, Germany) in combination with the petawatt PHELIX (Petawatt High Energy Laser for Heavy Ion eXperiments) laser system (Fig. 11b), which qualitatively extends the capabilities of this facility.

The capabilities and prospects of employing the GSI acceleration complexes are demonstrated in Fig. 12. One can see that high-intensity relativistic heavy-ion beams show good promise for the generation of high energy density plasmas and in the future, perhaps, for pulsed thermonuclear fusion [74, 170].

5.2 Relativistic collisions of nuclei. Quark–gluon plasma

As noted in the foregoing, high energy densities on record are being attained today in head-on collisions of heavy nuclei (see Fig. 10) accelerated to subluminal velocities in synchrotrons. These experiments are aimed at the experimental investigation of the basic problems of high-energy physics in hadron collisions which are attended with the production of superdense nuclear substance — quark–gluon plasma (QGP) (Figs 13a and 13b). In particular, unique experiments on the generation of an ultraextreme state of baryonic substance with a density of $\sim 10^{15}$ g cm^{-3}, a pressure of 10^{30} bar, and a temperature of ~ 200 MeV in Cu – Cu and Au – Au heavy-nuclei individual collision events were carried out at the CERN and Brookhaven accelerators. According to contemporary notions, this was precisely the state of the Universe's substance during the first microseconds after the Big Bang (Fig. 13c), and this is, perhaps, the state of the substance of astrophysical objects like gamma-ray bursts, neutron and quark stars, and black holes.

Of the huge amount of interesting physical data obtained using acceleration facilities, we enlarge here on the QGP generation which emerges in the deconfinement of quarks at energies $E \geqslant 200$ MeV [168, 181]. In the collision of two nuclei (see Fig. 10 [167]), the kinetic energy of motion is converted into the internal energy of the nucleons. This, in accordance with the predictions of quantum chromodynamics (QCD) [181], leads to the formation of a new state of matter: quark–gluon plasma, or 'quark soup' [168, 181] (Figs 13a and 13b).

The QGP emerging in this case consists of quarks, antiquarks, and gluons [182, 164, 183], possesses a maximal density of $\sim (9-10)\,\rho_0$ (where $\rho_0 = 2.5 \times 10^{14}$ g cm^{-3} is the nuclear density), and may emerge at the center of neutron stars and black holes or in the collapse of ordinary stars. The conditions attainable with contemporary accelerators are presented in the phase diagram of the nuclear substance (Fig. 13d).

Quark–gluon plasma is an essential element in the transformation of matter after the instant of origination of the Universe (see Section 6.5). During the first microseconds [164] after the Big Bang, the temperature decreased as T [MeV] $\sim t^{-1/2}$, where the time t is measured in seconds, so that the QGP with a temperature of several hundred MeV could exist during the first 5 – 10 μs after the Big Bang (Fig. 13e). That is why QGP is referred to as the 'oldest' form of matter.

Quark–gluon plasma [184 – 187] constitutes the superhot and superdense form of nuclear matter with unbound quarks and gluons which are bound inside hadrons at lower energies (Figs 13a and 13b). The existence of QGP follows from the property of asymptotic freedom of QCD [188 – 191], which yields a value of 1 – 10 GeV fm^{-1} for the energy density of a corresponding transition; this value is close to the energy density in the interior of a proton and exceeds the nuclear energy density by an order of magnitude. Detailed numerical calculations give the critical conditions for the emergence of QGP: $T_c \approx 150-200$ MeV, or $(1.8-2.4) \times 10^{12}$ K (Figs 13d and 13f).

The initiation of this plasma manifests itself in an increase in the number of degrees of freedom — from three inherent in the pion gas at low temperatures, $T < T_c$, to 40 – 50 inherent in the QGP for $T \sim (1-3)\,T_c$. Since the energy density, the pressure, and the entropy are approximately proportional to the excited degrees of freedom of the system, a sharp variation in these thermodynamic parameters in a small vicinity of T_c accounts for the large energy difference (up to ~ 10 relative units in Fig. 13f) between the ordinary nuclear substance and the QGP.

Like our customary 'electromagnetic' plasma, QGP may be ideal for $T \gg T_c$, and nonideal for $T \sim (1-3)\,T_c$. The corresponding nonideality parameter — the ratio between the interparticle interaction energy and the kinetic energy — in this case is given in the form $\Gamma = 2Cg^2/(4\pi aT) = 1.5-5$, where C is the Casimir invariant ($C = 4.3$ for quarks, and $C = 3$ for gluons), the interparticle distance $a \sim 1/T$ ($a \approx 0.5$ fm, $T = 200$ eV), and the strong interaction constant $g \sim 2$. The factor 2 in the expression for Γ takes into account magnetic interaction which in the relativistic case is of the same order of magnitude as the Coulomb interaction.

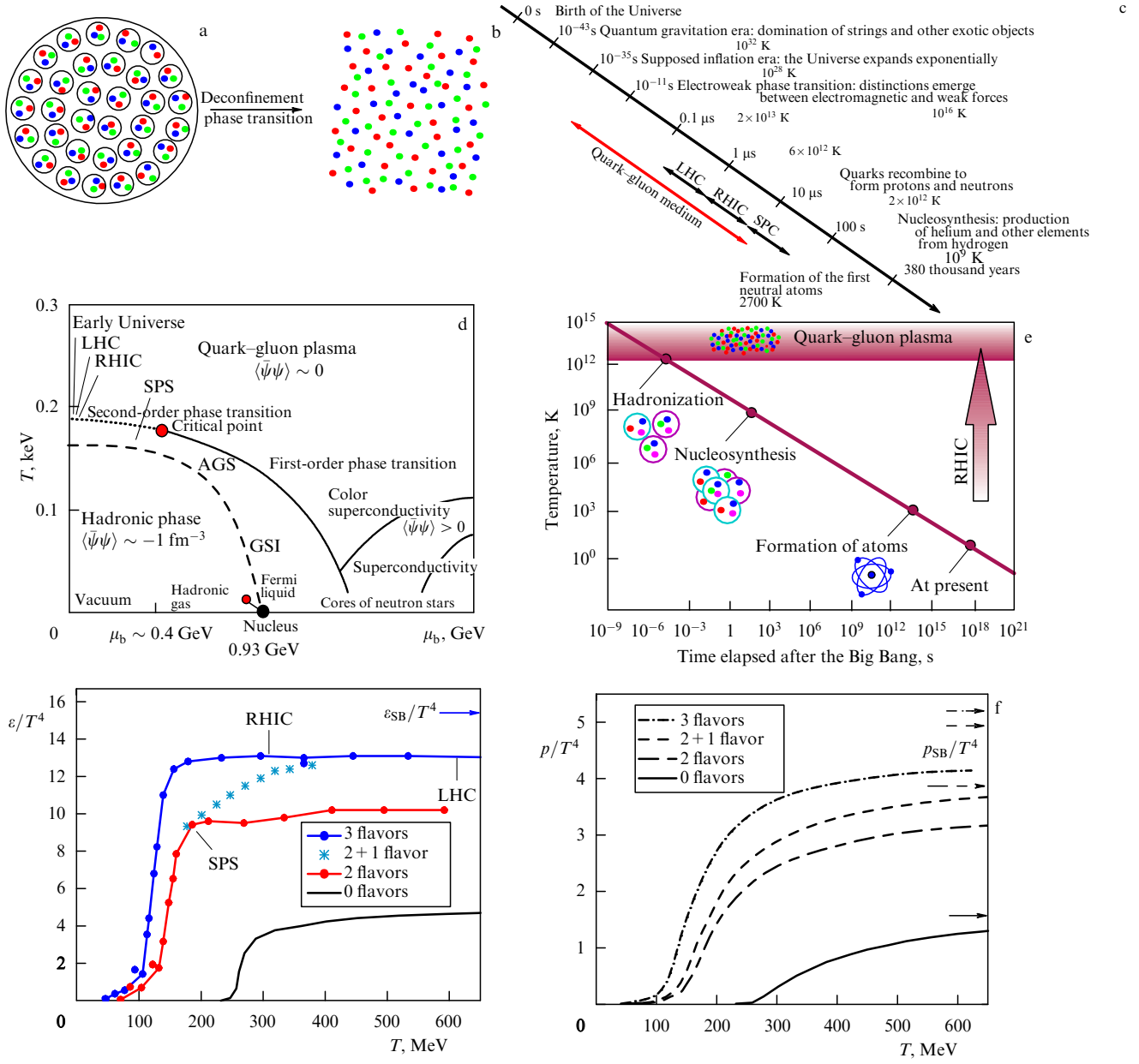

Figure 13. (a, b) Formation of quark–gluon plasma: (a) under ordinary conditions, quarks, which are indicated by points of different color, are bound inside hadrons; (b) for temperatures $T > T_c$ deconfinement of quarks occurs and they cease to be bound in hadrons to form QGP. (c) Cosmic time scale. Universe expansion after the Big Bang [167]. (d) Schematic phase diagram of quark–gluon plasma [197, 202]; AGS — Alternate Gradient Synchrotron. (e) Transformation of matter after the Big Bang. (f) Results of quantum-chromodynamic calculations of the temperature dependences of the energy density and pressure [168]. The most realistic case corresponds to 2 + 1 flavor; the subscript SB stands for Stefan–Boltzmann.

At present it is hard to tell unambiguously whether the transition to a QGP is a true thermodynamic phase transition with an energy density jump or a sharp and yet continuous transition [168]. In any case, the theory [168] predicts a low value for the speed of sound in the transition region, which is reflected in the hydrodynamic anomalies accessible to observations in the relativistic collisions of heavy nuclei.

The picture of relativistic heavy nucleus collisions is displayed in Fig. 10. Under the conditions of the RHIC experiment, the longitudinal Lorentzian shrinkage of the size of colliding nuclei is of the order of 100. The characteristic volume of the U – U collision region (≈ 3000 fm^3) contains $\sim 10{,}000$ quarks and gluons, while the characteristic collision time equals $\tau_0 \approx (0.2-2)\,\text{fm}/c \approx (5-50)\times10^{-25}$ s. That is why a part of high-energy processes supposedly proceeds in the expanding substance, when the nuclear bunches have already passed through each other.

During the collision, as the nuclear substance expands and cools down, the emergent quarks and gluons thermalize (the time $\tau_{eq} \leqslant 1\ \text{fm}/c \approx 3\times10^{-24}$ s) and may reach local thermodynamic equilibrium during the plasma lifetime $\tau_0 \sim (1-2)R/c \sim 10\ \text{fm}/c$, where R is the characteristic dimension of the plasma region. In this case, the medium will go into hydrodynamic motion; its recording may yield experimental information about the properties of the hadronic or quark–gluon substance or about the boundaries of their mutual transitions, which should occur at an energy density of ~ 1 GeV fm^{-3} according to quantum chromodynamics.

An analysis of the collision and expansion dynamics implies [168] that the transition from a relatively slow one-dimensional expansion to a faster three-dimensional expansion occurs in a characteristic time $t \sim 0.3$ fm/c. By the point in time $t \sim 3$ fm/c, the plasma comprises a mixture of quarks, gluons, and hadrons, and for $t \sim 10$ fm/c the quarks and the gluons recombine into hadrons. The lower bound of attainable energy density is realized for $t \sim 1$ fm/c, and the upper limit (massless gas) for $t \sim 0.3$ fm/c. The general estimate of the energy density W has the form [168]

$$(2-3)\ \text{GeV fm}^{-3} \leqslant W \leqslant (20-30)\ \text{GeV fm}^{-3}\,.$$

For comparison, the energy density in neutron stars (see Section 6) amounts to ~ 1 GeV fm^{-3}.

The formation of QGP should be accompanied by qualitatively new physical phenomena which should manifest themselves in experiments.

First, the emergence of new degrees of freedom in the plasma is reflected in collision and expansion relativistic hydrodynamics, which in turn is described by the equations of motion of a viscous fluid in the conditions of local thermodynamic equilibrium. The hydrodynamic formalism is simplified for a nonviscous fluid (the Euler equation), while the experimental manifestation of collective (viscous) effects may be indicative of plasma effects.

Second, the emergence of QGP manifests itself in the difference of parameters of hydrodynamic phenomena calculated from a given equation of state based on available experimental data.

Correlating the azimuthal flux components for π, K, ρ, and Λ in Au–Au collisions [192–196] shows that for energies up to 1 GeV fm^{-1} there is good agreement between the calculated and measured data, which is violated at higher energies. This disagreement is attributed to the emergence of QGP. Taking into account the lowering of the speed of sound in the vicinity of $T \approx T_c$, caused by the formation of this plasma, which leads to a 'softening' of the equation of state, would improve the correlation between the data of calculations and experiments.

The formation of QGP may show up not only in the indicated peculiarities of the equation of state, but also in the behavior of viscosity in the hydrodynamic motion. It is precisely these effects that are supposedly responsible for the lower (in comparison with calculations) elliptic expansion velocities measured at the SPS accelerator, this discrepancy being unavoidable in the framework of three-dimensional nonstationary (3+1)D hydrodynamics. In any case, ideal nonviscous flow calculations by the Euler equations [197] are in better agreement with experiments than are the calculations by equations with viscous dissipation.

The effects covering suppression of the jets produced in relativistic nuclear collisions also contain information about the properties of a shock-compressed substance [198–200] and the emergence of QGP. By the order of magnitude this suppression is determined by the radiative losses of gluons, while the contribution of elastic losses is relatively low.

These and several other experimental data permit determining the initial energy density W_0 in relativistic collisions:

$$W_0 \approx \frac{P_0^2}{\pi R^2}\,\frac{\mathrm{d}N_g}{\mathrm{d}y} \approx 20\ \text{GeV fm}^{-3}\,,$$

where $P_0 \sim Q_{sat}$. For the characteristic gluon momentum equal to 1.0–1.4 GeV, the formation time of the primary nonequilibrium QGP reaches $\tau \sim 0.2$ fm/c. Under these conditions, the local thermodynamic equilibrium required for the application of hydrodynamics will set in for $\tau_{eq} < 0.6$ fm/c. By this time the temperature will be $T(\tau_{eq}) \sim 2T_c$, where T_c is the calculated temperature for the emergence of QGP. According to one of the models [168], the number of minijets for $P_0 \sim 2-2.2$ GeV should be ~ 1000.

The jet suppression effects observed in nuclear collisions allow determining the energy density of the nuclear substance and drawing conclusions about the strong collective interaction (nonideality) of this plasma, proceeding from an analysis of the energy losses of the jets in their motion through the QGP.

As one of the elegant and interesting nuclear hydrodynamic phenomena, special mention should be made of the generation of conic Mach shock waves (Fig. 14): their properties, according to Stöcker's bright idea [201], permit judging the characteristics of a compressed nuclear substance.

The quark–gluon plasma and the ordinary plasma, which comprises 95–99% of the visible Universe and which is referred to as electromagnetic plasma (EMP), have many differences and yet share much in common [181]. Unlike the EMP, the quark–gluon plasma is relativistic or ultrarelativistic. This distinction in relativity shows up not only in the kinematics of motion, but also in the nonrelativistic case seeing only particles whose number is a conserved quantity, while the relativistic case also sees antiparticles and the number of leptons is a conserved quantity. The particle density is no longer an adequate characteristic of the QGP.

The most common feature of the QGP and the EMP lies in the collective nature of interparticle interaction [181]. Despite screening, the radius of effective electromagnetic interaction is normally much longer than the interparticle distance, so that there are many particles in the Debye sphere and their motion is strongly correlated. Quantum electrodynamics gives a solution for the pseudopotential, which corresponds to the Debye one:

$$\Phi(r) = \frac{q}{r}\,\exp(-m_D r)\,,$$

in which the Debye mass (its inverse quantity plays the part of the Debye radius in the atomic system of units) $m_D^2 = e^2T^2/3$ is of the order of $(qT)^2$, where q is the constant of quantum

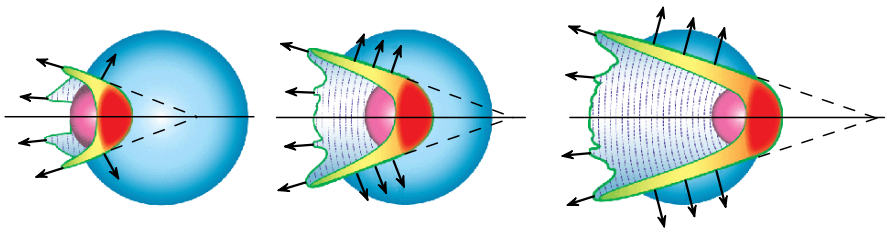

Figure 14. Generation of Mach shock waves in the nuclear substance [201] in the collision of a light nucleus (at the left) and a 'heavy' one.

electrodynamics. Since the number of particles n in this theory equals $\sim T^3$, the number of particles in the Debye sphere $N \sim 1/q^3$ in the weak-compression limit $(1/q \gg 1)$. Interestingly, the pseudopotential of the interparticle interaction of like charges in QGP may become attractive in some cases [181]. A consequence of the long-range interparticle interaction inherent in EMP and QGP is that an important role is played here by collective effects like screening, plasma oscillations, instability, etc.

In the experiments with EMPs, use is made of external electromagnetic or gravitational fields. Unlike EMPs, for QGPs the fields of requisite intensity are extremely high, and only self-induced fields are of significance in relativistic collisions of particles.

Many hydrodynamic and kinetic plasma instabilities typical of EMPs may presumably show up in the QGP as well [181], although they are extremely hard to observe there. However, the development of these perturbations is associated with a short ($\leqslant 1$ fm$/c$) measured QGP thermalization time and the effect of jet suppression in relativistic nuclear collisions.

Experimentally examined [181] fast substance thermalization, the parameters of elliptical streams, the spectrum of outgoing particles, jet suppression, and low viscosity are attributed [181] to the nonideality of QGP, which is near the deconfinement boundary. The above-given estimate $\Gamma \sim 1.5-5.0$ of the nonideality parameter may increase by an order of magnitude when higher-order terms in the interaction potentials are taken into account [181]. This in turn may give rise to a 'plasma' phase transition similar to that observed in a strongly nonideal nonrelativistic plasma [2, 4, 54].

Interesting analogies [181] are drawn between strongly nonideal QGPs and strongly nonideal dust plasmas [4, 40, 43]. In both cases, we are supposedly dealing with a non-Newtonian liquid, in which the shear viscosity depends on the velocity of motion. Furthermore, the QGP perhaps possesses the features of a nanoliquid [181]. In particular, the initial size of QGP immediately after a collision reaches ~ 10 fm (~ 20 interparticle distances), which distinguishes it from a continuous medium. This is also typical of a nonideal dust plasma [4, 40, 43].

Analogies between QGP and EMP may be a helpful aid in the elucidation of several fundamental properties of QGP, especially those which are hard to obtain from direct experiments on relativistic ion collisions.

6. Astrophysical aspects of high energy densities

High energy density physics underlies the contemporary understanding of the structure and evolution of astrophysical objects, which arise under the action of gravitational forces and thermonuclear energy releases [1]. The scale range and diversity of these phenomena are astounding, and comprehending them calls for the latest ideas and data from the cutting edge of modern physics.

Observations of astrophysical objects are carried out in a broad range of the electromagnetic spectrum from hard gamma-rays to meter waves, providing unique information about the physical processes at ultrahigh energies unattainable for modern accelerators. According to Ya B Zel'dovich's vivid statement, the Universe is "an accelerator for the poor" which does not demand from them multibillion expenses for the construction of experimental facilities.

Table 3. Characteristic parameters of matter in nature and in the laboratory.

Object	T, K	ρ, g cm^{-3}	p, bar
Intergalactic gas	10^7-10^8	$10^{-30}-10^{-3}$	$10^{-17}-10^{-7}$
Earth, center	5×10^3	10–20	3.6×10^6
Jupiter, center	$(1.5-3)\times10^4$	5–30	$(3-6)\times10^7$
Exoplanets	10^3-10^5	1–30	10^7-10^8
Diamond anvils	4×10^3	5–20	5×10^6
Shock waves	10^7	13–50	5×10^9
Controlled thermonuclear fusion, magnetic confinement	10^8	3×10^{-9}	50
Controlled thermonuclear fusion, inertial confinement	10^8	150–200	2×10^{11}
Sun	1.5×10^7	150	10^{11}
Red giant	$(2-3)\times10^7$	10^3-10^4	5×10^{12}
White dwarf	10^7	10^6-10^9	$10^{16}-10^{22}$
Relativistic collision of Au nuclei, 100 GeV per nucleon, Brookhaven	$2\times10^7-7\times10^{13}$	10^{15}	10^{30}
Neutron star, black hole, gamma-ray bursts	10^8-10^{11}	$10^{14}-5\times10^{15}$	$10^{25}-10^{27}$
Early Universe (Planck's conditions)	10^{32}	10^{94}	10^{106}

The range of matter parameter variations in the Universe is extremely broad [7, 10]: from empty space [2] and the rarefied intergalactic gas with a density of 10^{-30} g cm^{-3} to extremely high neutron star densities of $10^{14}-10^{17}$ g cm^{-3} (Table 3). The temperature of the intergalactic gas with a particle number density $n \sim 10^{-4}-10^{-3}$ cm^{-3} amounts to 10^7-10^8 K, but may range up to 10^9 K when heated by shock waves (arising from the shedding of stellar shells, stellar collisions and explosions, the collisions of gas clouds, etc.). Inside neutron stars, the temperature reaches 10^8-10^{11} K [1]. The greater part (99%) of visible matter is heated to temperatures exceeding 10^5 K.

While the magnetic field induction amounts to $\sim 10^{-9}$ G in intergalactic space and to 10^{-6} G near the galactic plane, at the surface of neutron stars it is 22 orders of magnitude higher. The record is held by the recently discovered magnetars — neutron stars produced upon supernovae bursts. Magnetars possess a magnetic field induction up to 10^{15} G, which corresponds to densities of order 10^8 g cm^{-3} approaching the density of nuclear matter [204, 205]. The gravitational accretion of matter gives rise to highly collimated jets, the beams of charged particles accelerated to ultrahigh energies. Supernovae explosions generate shock waves, plasma ejections, turbulent plasma and dust

[2] These parameters are derived from the measurements of gravitational effects in a vacuum and are consistent with the notions of the upper bound following from the constrains imposed from below on the curvature of space [203].

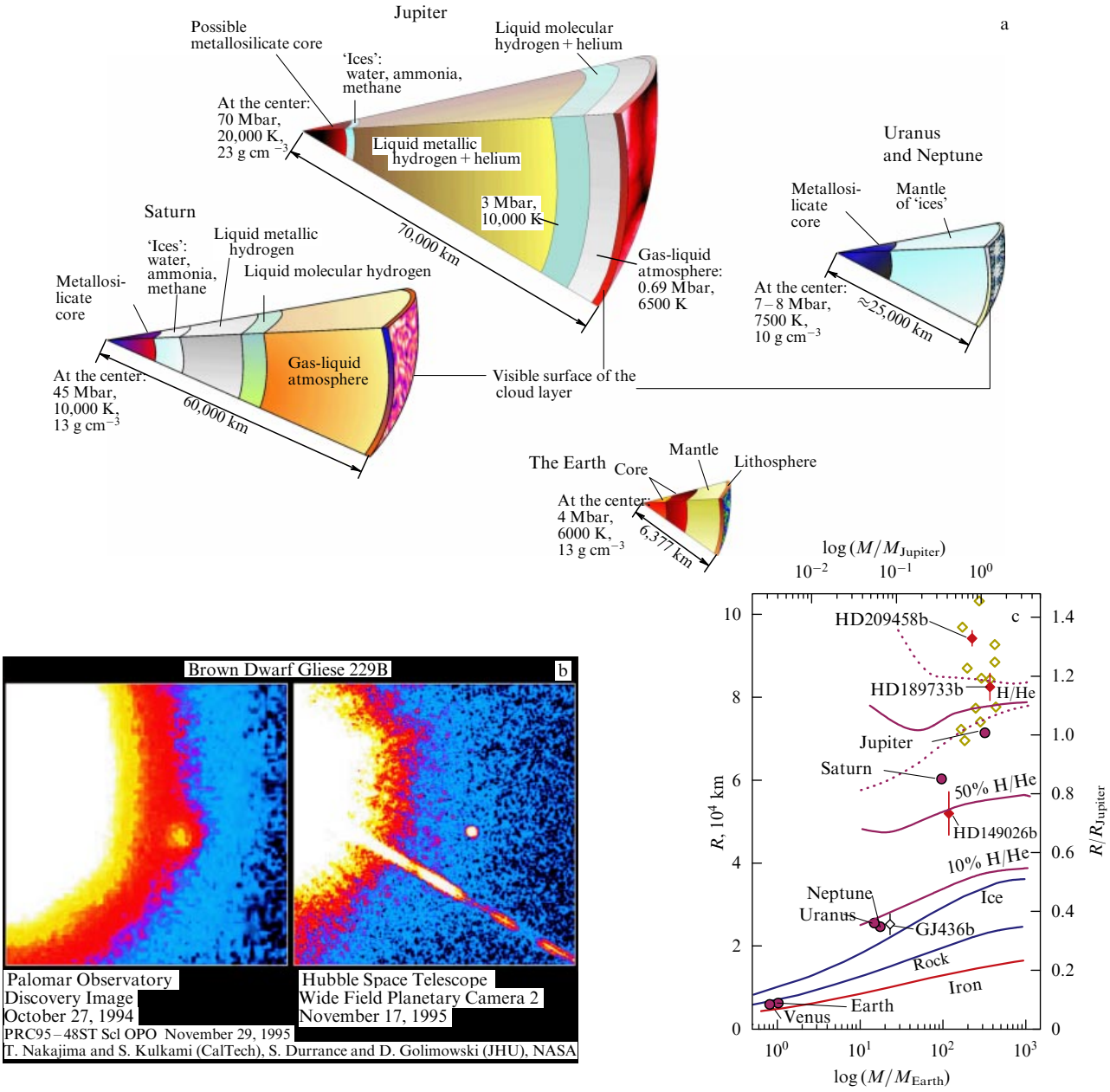

Figure 15. (a) Schematic of the internal structure of the giant planets in comparison with terrestrial structure [220]. (b) Photograph of a satellite of the star Gliese 229. The image was obtained by the Hubble Space Telescope [221]. (c) Characteristics and chemical composition of exoplanets in comparison with several planets of the Solar System [222].

clouds, producing the material for the formation of stars [5, 7, 8, 10]. Neutron stars measuring several kilometers rotate at kilohertz frequencies and act on the plasma with their gigantic magnetic fields to generate high-intensity X-ray radiation. Detailed astronomical observations testify to the predominance of new forms of matter like dark matter and dark energy. However, the structure of even the closest planets of the Solar System is as yet imperfectly understood.

The objective is to reproduce to some extent these exotic states and the transformations of matter in laboratory conditions by way of relativistic nuclear collisions, at the focus of ultrahigh-power lasers, in imploding plasma pinches, or in supercomputer simulations [5]. In this case, the difference in laboratory and astrophysical scales amounts to many orders of magnitude (up to 25), calling for the choice of adequate dimensionless variables and a careful analysis of similarity criteria [9, 60]. The existing and fundamentally possible technical capabilities, along with the prospects of high energy density cumulation, which were described in the previous sections, constitute the technical basis for laboratory astrophysics [9, 60, 206] — a rapidly developing field of high energy density physics.

Let us briefly, from only the standpoint of high energy density physics, consider several examples of astrophysical objects [5].

6.1 Planets, exoplanets, substars, white and brown dwarfs

Figure 15a displays the structure and characteristic parameters of several giant planets of the Solar System, which

harbor 99.5% of the mass of circumsolar substance. One can see that complex structures and diverse physical processes in compressed and heated substances are at issue, which researchers should learn to reproduce in laboratories and describe by the theoretical models of dense plasmas at megabar pressures.

Much less observational information has been gained about the planets that are outside of the Solar System. To date, more than 230 such objects have been discovered since 1992. Astronomers detect these objects from the lowering of stellar brightness at the instant of time the exoplanet is running between a star and the terrestrial observer ('eclipsing' method).

Figure 15b shows a rare picture of the exoplanet-satellite of the star Gliese 229 made by NASA's Hubble Space Telescope. The mass of this exoplanet is 20 – 60 times the mass of Jupiter.

Figure 15c presents the dimensions and masses of a number of giant planets and exoplanets, as well as their chemical composition in comparison with several planets of the Solar System.

To interpret the data of terrestrial and space measurements and to construct on their basis models of the evolution, structure, and energy characteristics of these objects demands reliable data about the physical properties of nonideal plasmas in the megabar pressure range.

Experiments on the multiple (quasiadiabatic) shock compression of hydrogen, helium, and their mixtures performed with pneumatic guns [12] and explosive throwing devices [3, 4, 11, 54] yield the requisite information about pressure-induced ionization [3, 4, 11, 22] and about the phase transition [54] in this plasma. The measurements suggest that the plasma phase transition takes place in the deuterium isentrope at $p \approx 1.2$ Mbar, and the pressure-induced ionization occurs in a similar pressure range for a plasma density of $0.5 - 1.0$ g cm^{-3}. This has permitted measuring the radius of Jupiter at which metallization occurs and shifting it towards greater radii [2, 207].

Close to planetary objects in dimensions are brown dwarfs, low-mass stars, and substars, in the interior of which nuclear reactions have been completed [208] due to the insufficient mass of these objects (commonly their masses are $0.07 - 0.09$ of the solar mass, and a size is comparable to that of Jupiter). These 'unsuccessful stars' range from Jupiter to the Sun in mass and consist of a hydrogen–helium degenerate or partly degenerate nonideal plasma with a pressure of about 10^5 atm at the center, while the plasma in white dwarfs is completely degenerate [209 – 212].

The optical properties of stellar plasmas are one of the central areas of the application of high energy density physics to astrophysics, because radiation determines the energy transfer inside the stars, as well as their evolution and observable luminosity, yielding the bulk of observational information about these objects.

As an example of the plasma calculations of this kind we give an analysis of the optical phenomena involved in the impact of the comet Shoemaker–Levi 9 on Jupiter [213, 214], which enabled determining more precisely the composition and structure of the Jovian atmosphere, revealing the shock acceleration effect in an exponential atmosphere, and interpreting the optical signals recorded on the Earth and by space probes.

In the transformation of a gravitationally unstable gas-dust cloud into a star titanic changes occur in the physical conditions of the matter: the density rises by 20 and the temperature by 6 orders of magnitude. The substance undergoes a series of transformations from the molecular and solid states to a superdense relativistic plasma state.

The principal energy source in the subsequent stellar evolution is thermonuclear combustion, which is responsible for the production of heavy elements and takes place in a strongly compressed substance at extremely high temperatures [215]. In the course of this combustion [216], hydrogen transforms into helium (10^6 K), which passes into carbon and oxygen at a temperature $T \sim (1-2) \times 10^8$ K. Carbon at $T \sim 8 \times 10^8$ K yields neon, sodium, and magnesium, and oxygen at $T \sim 2 \times 10^9$ K gives silicon and sulfur. A temperature $T \sim 4 \times 10^9$ K is required for transforming silicon into iron and the neighboring elements. Here, the thermonuclear combustion terminates, because additional energy deposition is required for the production of heavier elements. These elements (Cu, Sn, Ag, Pb, Th, U) are synthesized through neutron capture reactions in explosions of type II supernovae and red giants.

Figure 16. New star explosion dynamics [217, 218].

The picture of the evolution and hence the parameters of plasmas in single stars depend strongly on their masses [8].

Figure 16 depicts the explosion dynamics of a new star [217, 218] in circumstances where the Chandrasekhar limit was not reached by way of accretion on it, resulting in a weaker explosion than in the case of a supernova.

A higher-power process is attended with a type II supernova burst (if an extended hydrogen shell has been retained) or that of a type Ib/c. In this case, the brightness of such a supernova is extremely high and may exceed the total brightness of all the rest of the stars in the Galaxy. Later on, for several dozen thousand years the remnants of the dumped shell persist in the form of a luminous nebula — a supernova remnant.

Accretion onto white dwarfs [211], which are quite interesting astrophysical objects from the standpoint of realization of extreme conditions, may lead to type Ia supernovae. In the evolution of stars of mass $(8-10)\,M_\odot$, the thermonuclear combustion terminates at the stage of a helium or carbon–oxygen degenerate core. Interestingly, in this case positive ions form a crystal lattice [8], which is a kind of a phase transition in a nonideal plasma [22, 37–40, 44, 48–54].

The energy parameters of stellar explosions vary greatly. For the 'weakest' astronomical explosions — solar flares — the time scale is about 10^3 s and about 10^{32} erg is released in this case. For novae, $t \sim 10^8$ s and the corresponding released energy $E \sim 10^{45}$ erg. For supernovae, $t \sim 10^{10}$ s and $E \sim 10^{50}$ erg. In galactic nuclei, it is likely that $t \sim 10^{15}$ s and $E \sim 10^{65}$ erg.

In several scenarios of stellar evolution (a supernova, a nova), thermonuclear combustion emerges in the inner domains of a degenerate plasma and is then transferred to the outer regions in the form of a wave of thermonuclear combustion (or thermonuclear detonation) or by way of convection. In this case, convective instabilities develop, resulting in the explosion of the object [219]. Similar convective processes, though without local thermonuclear energy liberation, supposedly take place in the outer regions of brown dwarfs as well. Unfortunately, convective phenomena in degenerate plasmas have not been adequately studied [5], which invites staging corresponding laboratory experiments.

It is hoped that the future NIF and MJL facilities will radically broaden the attainable range of parameters and enable reaching the conditions typical of terrestrial group planets, exoplanets, giant planets, brown dwarfs, and intermediate-mass stars, as well as of the outer layers of white dwarfs.

6.2 Superextreme states, neutron and quark stars, black holes, magnetars, and wormholes

Depending on the initial mass of a star of solar chemical composition, three types of compact remnants may emerge in the stellar interior upon completion of thermonuclear evolution: white dwarfs, neutron stars, and black holes [1, 8].

Perhaps the most exotic astronomical objects are neutron stars in which a broad spectrum of superextreme states of matter [223, 224] virtually unattainable for laboratory research is achieved. That is why neutron stars in a sense fulfill the function of a 'cosmic laboratory' — their observable manifestations permit judging the behavior of matter under superextreme conditions: at supernuclear densities, in superstrong magnetic fields, for the superfluidity of the baryonic component, and intensive nuclear transformations of ultracompressed matter. It is reasonable that the observable manifestations of these processes are also highly diversified: these are radio and X-ray pulsars, flaring X-ray sources, X-ray transients, magnetars, and so forth [8, 223, 225].

Neutron stars, which are associated with short-period radiation sources — pulsars — present the final (after a supernova explosion) stage of the evolution of ordinary stars with $M > 8\,M_\odot$, when gravitational forces compress their substance to nuclear densities (10^{11} g cm^{-3}) to produce neutron substance [1, 8, 226], which was predicted by L D Landau back in 1932.

The thermonuclear burning of ^{32}Si with the production of the iron isotopes ^{56}Fe, ^{58}Fe, ^{60}Fe, as well as of ^{62}Ni, etc. closes the chain of thermonuclear reactions in the nondegenerate core of a massive star. The density at its center amounts to 3×10^9 g cm^{-3} for $T \sim 8 \times 10^9$ K and a core mass of $1.5-2\,M_\odot$ [8]. Important processes stimulating the gravitational collapse are the photodissociation of iron nuclei into 13 alpha particles:

$$\gamma + {}^{56}_{23}\mathrm{Fe} \rightarrow 13\,{}^{2}_{4}\mathrm{He} + 4\mathrm{n}\,,$$

and the substance neutronization.

According to the Pauli exclusion principle, the neutron substance is stable against neutron decay by the scheme

$$\mathrm{n} \rightarrow \mathrm{p} + \mathrm{e}^- + \bar{\nu},$$

because the energy level of an electron that might be emitted in the decay is already occupied by other electrons which enter into the composition of the substance. In the upshot, as the compression becomes stronger a progressive speed-up of the process occurs involving the electron capture by nuclei with the transformation of protons to neutrons. Such a star resembles one atomic nucleus of tremendous size.

A specific feature of neutron stars is their superhigh (nuclear) density of order 2.8×10^{14} g cm^{-3}. However, unlike an atomic nucleus, in which nucleons are held together by a strong interaction (quarks), nucleons in a neutron star are held by gravitational forces, while the neutron β-decay is suppressed by the strong electron degeneracy of the compressed substance.

The elasticity of a degenerate substance lowers in the neutronization [8], because the electron number density decreases with retention of the baryon density, the substance becomes 'softer', and the collapse of the cores of massive stars takes place at later stages of their evolution.

An additional cause of the loss of hydrostatic stellar stability arises from the general relativity effects: the substance pressure makes a contribution to the attractive force to increase the force tending to compress the substance [1, 226]. In this case, the collapse of the core of a massive star is attended with a type II or Ib/c supernova burst.

The collapse of the stellar core terminates at densities of the order of the atomic nucleus density, whereby the effects of neutron degeneracy become significant and the substance's compressibility becomes capable of resisting the action of gravitational forces.

Eventually, a compact star with $M \sim M_\odot$ forms, only about 10 km in size, with an initial temperature of 10^{11} K and a core density reaching $(1.5-15)\,\rho_0$ ($\rho_0 = 2.5 \times 10^{14}$ g cm^{-3} is the nuclear substance density; see Fig. 13d). The star possesses strong magnetic ($B \sim 10^{11}-10^{16}$ G) and gravitational (accel-

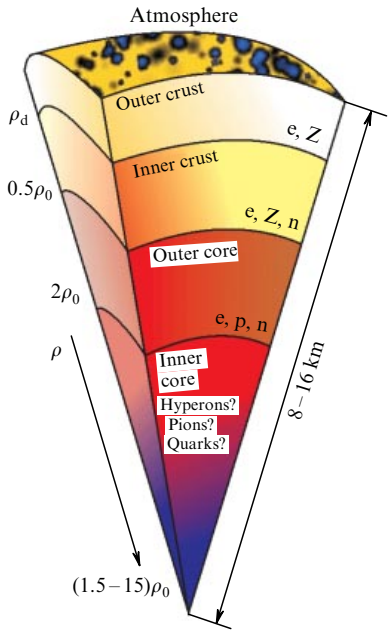

Figure 17. Schematic cut of a neutron star of mass $1.4\,M_\odot$. The stellar parameters depend greatly on the equation of state of its layers [8, 223]; $\rho_0 = 2.8 \times 10^{14}$ g cm^{-3}, and $\rho_d = 4 \times 10^{11}$ g cm^{-3} (different sources give somewhat different values for the latter quantity).

eration of gravity amounting to $(2-3) \times 10^{14}$ cm s^{-2}) fields, which necessitates employing the general theory of relativity for its description. Neutron stars rotating with a period of 0.0016 – 1 s (radio pulsars) make up the only astrophysical objects in which the mechanism of rotation moderation (and hence the evolution) is determined by electrodynamic forces. Neutron stars that are the parts of binary systems manifest themselves as compact X-ray sources [8].

Despite the small size of a neutron star, the spectrum of substance states (Fig. 17) and the physical processes in a neutron star are immensely diversified.

The atmosphere of a neutron star ranges from tens of centimeters to several millimeters in thickness and has a density of 0.1 – 100 g cm^{-3}; it consists of a nonideal plasma with $T \leqslant 10^6$ K and possesses a giant magnetic field. In a number of cases, the magnitude of this field is sufficient for spontaneous electron–positron pair production [227].

The outer crust several hundred meters in thickness [223], consists of a dense plasma in which the electrons pass from the Boltzmann state to the degenerate state as they travel toward the interior, and then (for $\rho \gg 10^6$ g cm^{-3}) to the state of a degenerate relativistic gas. For $\rho \geqslant 10^4$ g cm^{-3}, complete pressure-induced ionization of plasma occurs. On further compression, β-capture and substance neutronization are involved.

At the boundary with the core of a neutron star ($2\rho_0 < \rho < 20\rho_0$), atomic nuclei vanish and the neutrons in the inner crust may be superfluid, which is reflected in the cooling dynamics and on the neutron luminosity of the object. Since the stellar temperature depends crucially on the critical temperature of nucleon transition to the superfluid state, Page and Applegate [228] came up with the idea of using a neutron star as a 'thermometer' for measuring the critical temperatures of nucleons in asymmetrical nuclear matter, which may yield indirect information about the equation of state of the nuclear substance.

The inner core composition of a neutron star is not exactly known owing to insufficient knowledge of the physics of strong interactions in superdense substances [1, 8]. It is not unlikely that the core consists of a nucleon–hyperon substance, pion condensate, quark–gluon plasma, or some other exotic states. According to Yakovlev et al. [223], if the properties of the neutron star crust ($\rho < 0.5\rho_0$) are described by nonideal plasma models, then for $\rho \geqslant \rho_0$ the description of the properties of a supernuclear-density substance is severely hampered by the incompleteness of laboratory data and the absence of a complete theory of supernuclear-density substances [45, 46].

When a magnetic field trapping takes place in the course of evolution, a neutron star becomes a magnetar [229] — a star possessing a superhigh (up to 10^{15} G) magnetic field [229]. For the SGR 1806-20 magnetar, the highest-power magnet in the Universe, the measured magnetic field turned out to be record breaking: $\sim 10^{15}$ G, which corresponds to a density of order 10^{13} g cm^{-3}, approaching the density of nuclear matter. It is likely that in a number of cases QGP may come into being in the central regions of neutron stars (see Section 5.2). These objects are referred to as strange quark–gluon stars [168].

Superdense states of matter and, in particular, QGPs may also show up in black holes — objects predicted by the general theory of relativity, wherein the gravitational field is so strong that the escape velocity from the hole is equal to the speed of light [10, 230]. A black hole represents a space–time domain with a distinguished event horizon — a surface of size $r_{BH} = 2gM/c^2 \sim 3M/M_\odot$ [km], from under which no information may come out and become accessible to an external observer. The prerequisite to the occurrence of black holes is ultrastrong substance compression: $r_{BH} \sim 3$ km for the Sun, $r_{BH} \sim 1$ cm for the Earth, and $r_{BH} \sim 0.12$ mm for the Moon.

For the Earth ($M = 3 \times 10^{-6} M_\odot$), the critical density is extremely high: 2×10^{27} g cm^{-3}, by 13 orders of magnitudes larger than the atomic nucleus density.

The accretion of a substance of a neighboring star onto a black hole is attended with a tremendous energy release in the X-ray range with a luminosity of $\sim 10^{36} - 10^{39}$ erg s^{-1}, which is several million times higher than the bolometric luminosity of the Sun. Thus, the optical star plays the role of a probing body in the gravitational field of a relativistic object. In this case, black hole candidates differ from neutron stars not only by their greater mass (by more than a factor of three) and the absence of a magnetic field, but also by observable manifestations: these high-power X-ray radiators are neither X-ray pulsars nor type I X-ray bursters [7, 183, 230]. The radiation intensity of these objects ranges up to gigantic values of 10^{27} W cm^{-2}, which exceeds the highest value attained for focused laser radiation by six orders of magnitude (see Table 2). For a typical black hole with a mass $M = 10\,M_\odot$ and a supernuclear density $\rho \sim 10^{16}$ g cm^{-3}, available models suggest that the pressure of substance in it is at a level of $(2-3) \times 10^{24}$ Mbar.

It is significant that the last instants prior to the disappearance of a black hole will pass in the regime of a high-power explosion with an energy release of order 10^{30} erg in a time of about 0.1 s. Such explosions might be observable at a long distance from the Earth.

It is not unlikely that at the centers of quasars there are black holes with masses of $\sim 10^8 M_\odot$, which accounts for the high-power radiation emanating from the polar regions of quasars [231].

It is likely that supermassive black holes (with $M > 10^5 - 10^{10} M_\odot$) are the central elements of a number of galaxies [8].

An important feature inherent in relativistic astrophysical objects is the existence of gigantic magnetic fields which determine to a large measure the dynamics of their motion and radiative characteristics.

In the analysis of observational data it is highly important to have ideas about the physical properties of the partially ionized dense plasma residing in the outer layers of a neutron star in the presence of intense magnetic fields ($B \sim 10^{11} - 10^{16}$ G) [224, 225].

It is common knowledge that strong magnetic fields radically change the properties of a substance. In particular, the equation of state for $H \approx 150$ MOe becomes much more rigid. For $B \sim 10^{12}$ G, the pressure of a magnetic field at the surface of a neutron star amounts to about 40 Pbar. For the magnetic field induction

$$B \gg B_0 = \frac{m_e^2 e^3 c}{\varepsilon^2 \hbar^3} \sim 2.35 \times 10^9 \text{ G}$$

(ε is the permittivity), the cyclotron electron energy given by

$$\hbar\omega_e = \hbar \frac{eB}{m_e c} \approx \frac{11.58B}{10^{12}} \text{ [keV]}$$

is much higher than the electron–nucleus Coulomb interaction energy. Under the conditions of a neutron star, the Coulomb force represents a weak perturbation with respect to the magnetic one, and for typical stellar temperatures the electrons reside at the Landau level [7, 224]. Since the motion of atoms and ions is restricted in the direction perpendicular to the magnetic field, they assume a cylindrical shape and have high binding energies [232, 233]. Furthermore, when an atom moves in a constant magnetic field, due to the Lorentz transformation an electric field emerges in the intrinsic frame of reference, which may ionize the system [232, 233]. Much is still unclear in the structure as well as in the electronic and mechanical properties of such exotic states of a strongly magnetized substance [5, 224].

Describing the radiation transfer in ionized plasmas with $T > 10^6$ K and magnetic fields $B > 10^{14}$ G involves certain difficulties related to the polarization of a vacuum and virtual electron–positron pair production [227] in ultrahigh magnetic fields

$$B > B_c = \frac{m_e^2 c^3}{e\hbar} \approx 4.4 \times 10^{13} \text{ G},$$

which change the dielectric properties of the medium, polarize the proton motion, and thereby change the radiative plasma properties.

Even today, new-generation superhigh-power short-pulse lasers generate fields of order 10^9 G in laser-produced plasmas (see Refs [131, 134] and Section 4). The advancement of laser research may provide new information about the radiation capacity and spectra of astrophysical plasmas in strong magnetic fields.

Recently, one more mechanism of the origination of black holes related to the collapse of so-called magnetic tunnels or wormholes [235, 236] has come under discussion [234]. These highly exotic objects supposedly emerged at the early stages after the Big Bang and have persisted for various reasons until the present time. According to the chaotic inflation model,

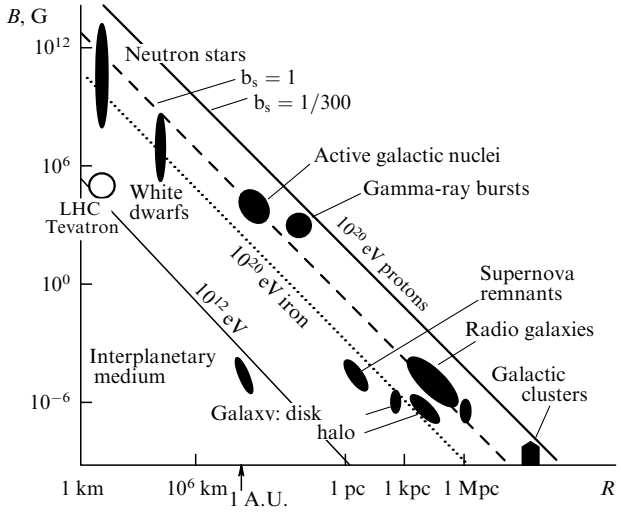

Figure 18. Hillas diagram showing the characteristic magnitudes of magnetic field induction and dimensions of astrophysical objects [237] (b_s is the velocity reduced to the speed of light).

which underlies modern cosmology [234], there may exist an infinite number of other universes which originate in a scalar field in different spatial domains and at different points in time to make up the so-called spatio–temporal foam [235, 236]. Some parts of our Universe and other universes may be connected by traversable spatio–temporal tunnels — wormholes — which existed in the initial scalar field and have persisted after inflation.

Wormhole parameters correspond to ultrahigh energy densities which may be comparable to those in the immediate spatio–temporal vicinity of the Big Bang [234]. Attention is drawn to the extremely high magnetic fields induced by these objects. For the fields

$$B = \frac{m_e^2 c^3}{e\hbar} \sim 4.4 \times 10^{13} \text{ G},$$

the spacing between Landau levels exceeds the electron rest energy. Positronium atoms acquire stability for $B > 10^{24}$ G, being spontaneously produced in a vacuum to fill the entire medium. The breakdown of the vacuum and the monopole pair production take place when $B \sim 2.6 \times 10^{49}$ G, leading to a wormhole mass of only 1.8 kg, which is supposedly the lower bound for the mass of these objects.

Figure 18 depicts a Hillas diagram with the characteristic magnitudes of magnetic field inductions and dimensions of astrophysical objects [237]. It also demonstrates their capabilities as particle accelerators. Solid lines represent estimates of dimensions R and magnetic field inductions B of the objects capable of accelerating protons to energies of 10^{20} and 10^{21} eV for a shock wave velocity 300 times lower than the speed of light. The dotted line represents the same for iron nuclei. Dark spots indicate the observed dimensions and magnetic fields of different astrophysical objects. Shown for comparison are the characteristics of the Tevatron and LHC accelerators. It seems likely that under the assumptions made about the particle acceleration mechanism (Fermi) itself there are no obvious candidates, in the Universe known to us, for the role of a Zevatron accelerator — the particle accelerator for energies close to the energy of observed cosmic particles.

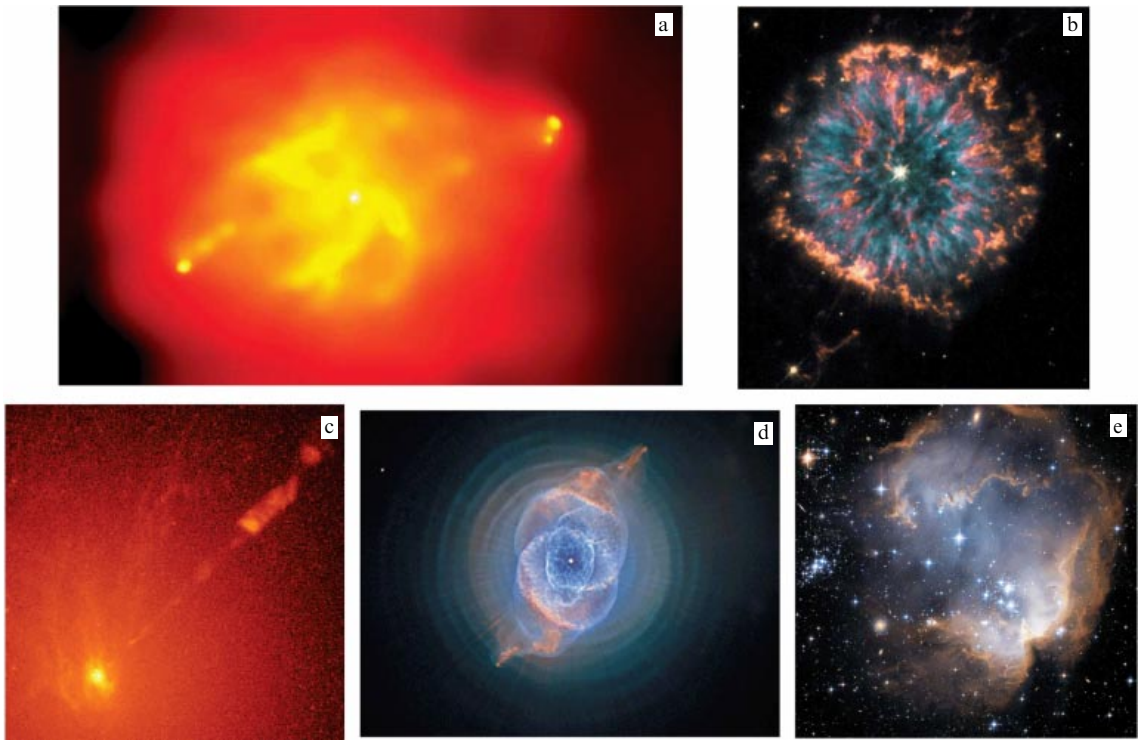

Figure 19. (a) Accretion of a substance onto a black hole [9] in the galaxy Cygnus A: one can see cosmic jets responsible for high-power X-ray and radio radiation. Under deceleration due to the ambient medium, they produce 'hot spots' and gigantic cavities. The radio emission power of Cygnus A is about 10^{45} erg s^{-1}, which is approximately 10 million times the emission power of the Andromeda galaxy. (b) Planetary nebula NGC 6751 in the Aquila constellation: one can see the gas streams escaping from the central star (photo from the Hubble Space Telescope) [247]. (c) Jet formation in the accretion of a substance onto a massive object [9] at the center of the galaxy M87. The jet consists of high-velocity particles and exhibits a structure of inhomogeneities (nodes) measuring ~ 10 light years. (d) Cat's Eye nebula (NGC-6543) [218] located 1 kpc away from the Sun. Seen at the center is a remnant of a star which shed its plasma shells (photo from the Hubble Space Telescope). (e) Newborn stellar cluster (region N90) surrounded by the residual gas from which it was formed [247].

6.3 Cosmic jets, radiative shock waves, molecular clouds, and cosmic rays

High-power ($\sim 10^{39}$ W), lengthy (0.01 – 2 pc long), and well-collimated (with divergence angles of 5 – 20° and sometimes even less than 1°) differently directed molecular and plasma relativistic jets (with velocities of up to $0.9c$) are observed in many active galaxies, quasars, and old compact stars [5, 8, 10, 238] (Fig. 19). In the case of the most active quasars, these jets are often attended with electromagnetic radiation of a wide frequency range — from radio-frequency emission ($\sim 10^8$ Hz) to superhard gamma-ray radiation (10^{27} Hz). Well-collimated jets with velocities of 100 – 300 km s^{-1} are also characteristic of many young stars.

Observations and theoretical analysis reveal that the magnetic fields rotating together with accretion disks accelerate and focus these plasma jets, the fields extracting the energy from the accreting masses or from the rotating black holes.

Laboratory experiments on plasma jets in collisional and collisionless regimes may be carried out on high-current Z-pinch facilities. The energy exchange and the generation of radiation and shock waves may be studied in the collisional regime. By lowering the density of targets it is possible to model the penetration of the jets into the targets, their dynamics, and thermalization.

Thus, the use of Z-pinches and lasers [9] has enabled obtaining hydrodynamic plasma jets with Ma $\approx 5-10$ and strongly radiating jets with Ma $\approx 50-60$ [5, 239] in laboratory conditions. A new class of high-energy, electroneutral, and well-collimated proton jets with an energy of up to 100 MeV was produced employing picosecond terawatt lasers [26, 27, 57 – 59, 127, 240].

Gigantic pulsed energy releases in astrophysical objects are inseparably linked with the massive plasma ejections, the generation of intense shock waves, solitons, and contact surfaces in cosmic plasmas [5, 8 – 10] (Fig. 19d), which may be caused by a supernova explosion, stellar wind, a galactic spiral wave, the mutual collision of clouds and stars, etc.

In dense molecular clouds [5, 8, 10], the temperatures of shock-compressed plasmas range into the tens of millions of degrees. These waves are subject to radial oscillations if their cooling time increases slowly with temperature. Furthermore, dense cooled regions are also sometimes longitudinally unstable.

Interstellar space is not empty or uniform — it is filled with a low-density substance, radiation, and a magnetic field with the corresponding characteristic energy density of ~ 1 eV cm^{-3}. On average, one cubic centimeter of interstellar space contains no more than one hydrogen atom and many fewer other chemical elements. In one cubic kilometer of this space there are no more than ten specks of dust measuring one micrometer each. The substance temperature varies here over wide limits — from 10 K to 10^6 K. Dense gas and dust regions have come to be known as clouds (or nebulae); they are 100 – 300 pc in size, up to $10^7 M_\odot$ in mass, and are classed into diffuse ($T \sim 10^2 - 10^3$ K, $n \sim 1 - 10^2$ cm^{-3}), dark ($T \sim 10 - 10^2$ K, $n \sim 10^2 - 10^4$ cm^{-3}), molecular ($T \sim 5 - 50$ K, $n \sim 4 \times 10^2 - 10^6$ cm^{-3}), and globular

($T \sim 10-30$ K, $n \sim 10^3-10^6$ cm^{-3}). It is likely that some of them came into being in the regions of active star formation, and the emergence of molecules in turn is an indication that the medium has cooled down, has become denser and is ready for star formation [241].

The jet dynamics of dust clouds and dust disks are influenced by the fact that the specks of dust may be charged (owing to photoionization) and form the so-called dust plasma [40] which possesses many unusual properties including, as evidenced by experiments, anomalous viscosity (for more details, see reviews [40, 43]).

The study of molecular and dust clouds in laboratory conditions may be carried out with the aid of high-power lasers and high-current devices, which model the ablation dynamics of clouds, the stability of interfaces, and the effect of radiation on the structure and development of radiative hydrodynamic instabilities. Furthermore, the generation of shock waves in such media may give rise to substantial nonuniformities and the development of turbulence. Research in the generation of laser-driven shock waves and of compression waves with Z-pinches is now in progress [9, 16, 70–72] and may yield a wealth of new information for the understanding of formation mechanisms of molecular clouds in space.

Nonstationary magnetodynamic phenomena, which determine stellar activity, present an interesting problem.

Magnetohydrodynamic phenomena on the Sun have been studied, of course, most thoroughly [242]. Continuous observations are made of magnetic instabilities and the reconnection topology of magnetic field lines on the solar surface. The dynamics of motion and compression of magnetic flux tubes is quite often nonstationary and explosive in character, and the magnetic field induction amounts to 3–4 MG in sunspots for an average magnitude of about 1 G. The temperatures in solar flares amount to 10^8-10^9 K, while the plasma parameters in the solar interior are as follows: $T \sim 1.5 \times 10^7$ K, $\rho \sim 150$ g cm^{-3}, and $p \sim 0.2$ Tbar; the time of photon diffusion from the core to the solar surface reaches $\sim 10^5$ years. Laboratory experiments supplemented with three-dimensional simulations [243, 244] provide a basis for the explanation of complex phenomena of field self-organization in magnetoactive plasma.

It is significant that suchlike effects of local energy cumulation give rise to global solar oscillations which are recorded with a very high degree of accuracy (to hundredths of one percent). The characteristics of these oscillations depend on the composition and thermodynamic properties of the solar plasma, which yields a unique high-precision experimental material for verifying multicomponent plasma models and defining more precisely the elemental composition of solar plasma [245]. In this case, the Sun fulfills the function of an 'experimental' facility for studying nonideal plasmas.

The energy of cosmic rays, which provide another example of extremely high energies in space, ranges from several kiloelectron-volts to 10^{20} eV. Cosmic rays are inherently a strongly rarefied relativistic gas whose particles only slightly interact with each other, and possess a power-law energy spectrum rather than the Maxwellian one. Cosmic rays undergo collisions with the particles of the interstellar medium and interact with the interstellar magnetic field. Although the cosmic ray flux near the Earth is low (~ 1 particle per cm^2 per s), its energy density (~ 1 eV cm^{-3}) is comparable to the density of electromagnetic radiation from all galactic stars, to the energy density of the thermal motion of interstellar gas and the kinetic energy of turbulent motion, or to the energy density of the galactic magnetic field [246]. The flux of superhigh-energy particles is extremely low: about 1 particle per km^2 in 100 years, but it is the origin and propagation of precisely these particles that has aroused the greatest interest.

6.4 Gamma-ray bursts

In modern astrophysics, gamma-ray bursts represent the most mysterious objects [5, 7, 8] with record energy releases since the Big Bang.

The relativistic 'fireball' model proposed for gamma-ray bursts in Refs [248, 249] reduces to the following: as a result of the collision (coalescence) of two neutron stars (Fig. 20) [250] or the gravitational collapse of a supermassive star, a 10^{52} erg energy release occurs in a small region filled with relativistic photons and leptons with a small admixture of baryons. This 'fireball' with an initial temperature of 1–10 MeV expands with a relativistic velocity and generates gamma-ray radiation by electrons accelerated by the Fermi mechanism in optically thin shock waves. A small number of baryons are also accelerated to relativistic energies and carry away a part of the energy from the fireball, generating outside of it outward and backward shock waves whose X-ray radiation is recorded as a gamma-ray burst. A substantially longer X-ray afterglow results from diverging shock waves. The ordinary duration of this radiation equals $\gtrsim 2$ s.

The typical density of the substance in accretion disks and jets is $\rho \gtrsim 10^{14}$ g cm^{-3}, which corresponds to the density of nuclear matter or neutron stars. As the fireball expands, inelastic nuclear collisions increase in importance and the relative velocity of neutrons and protons becomes comparable to the speed of light. Inelastic n- and p-collisions produce charged pions, gigaelectron-volt muons, and electronic neutrinos, which may be detected by spacecraft [5]. Powerful relativistic jets from gamma-ray bursts correspond to Lorentz factors $\gamma \geqslant 100$ and extremely high energy fluxes ($10^{50}-10^{52}$ erg s^{-1} or $10^{43}-10^{45}$ W). The energy density in the jet core (of the order of 10^{30} erg cm^{-3}) is sufficient for the spontaneous production of electron–positron pairs or initiation of nuclear reactions [1, 5, 7].

Tera–petawatt short-pulse lasers (see Section 4), which produce intensities of 10^{20} W cm^{-2} at a target, are best suited to the laboratory modeling (at least partial) of astrophysical processes. Impressive results have already been obtained in this area: well-collimated MeV-proton beams [57–59, 128–130], electron and positron beams with energies of 100 MeV

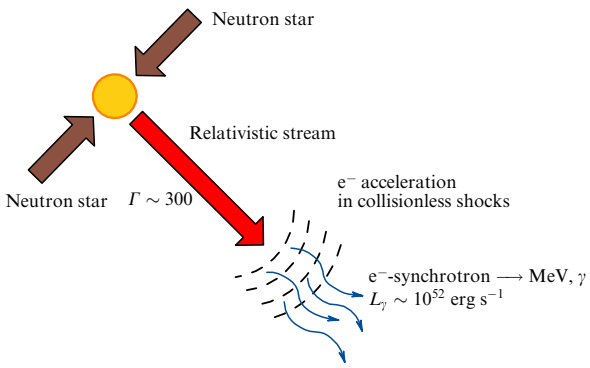

Figure 20. Gamma-ray burst scenario with 'fireball' formation [246].

[61, 63, 119, 122], thermally relativistic plasma with $T_e > m_e c^2$, which corresponds to the fireball conditions, as well as superstrong magnetic fields [26, 27, 131, 134, 136, 137]. These extreme plasma parameters are already approaching the parameters of gamma-ray bursts.

As noted in Section 4, the advent of petawatt lasers opens up new avenues for the production of relativistic and electron–positron plasmas in a laboratory. At intensities $\gtrsim 2 \times 10^{18}$ W cm^{-2}, these lasers produce nonthermal electrons with an energy $k_B T > m_e c^2$ in laser plasmas [23 – 25, 27, 42, 122, 251]. Electron–positron pairs [61, 63, 161] emerge in the interaction of these electron streams with heavy targets by the Bethe–Heitler mechanism.

The laser-produced electron–positron plasma may also be employed for modeling episodical annihilation phenomena in the neighborhood of black holes. In the two-sided irradiation of a gold target, two megajoule 0.1-petawatt lasers with a pulse duration of ~ 10 ns are capable [5] of producing a pair density which is several hundred times the electron background density. This would allow verifying the theoretical limitation, $k_B T \approx 20\, m_e c^2$, predicted by the theory of Zel'dovich, Sunyaev, and Bisnovatyi–Kogan [252, 253].

A significant part in the description of supernova explosions is assigned to numerical simulations involving one-, two-, and three-dimensional codes [9, 254, 255]. These calculations are based on the following assumption: as a result of gravitational stratification, the initial supernova structure (prior to the explosion) consists of the outer hydrogen layer, then a helium layer, and so on up to the iron inner core. The gravitational collapse of this inner core gives rise to a radially diverging intense shock wave which has high parameters at the helium–hydrogen interface: $\rho \sim 2.3$ g cm^{-3}, $T \sim 6$ keV, $p \sim 75$ Gbar, and leads to the development of the Richtmyer–Meshkov instability [62, 254 – 256].

Remington et al. [257] employed a Nova laser to model a supernova explosion in the laser-to-soft-X-ray radiation conversion scheme. X-ray radiographic measurements enabled tracing the stages of a nonlinear development of instabilities and comparing them with the data of numerical simulations.

It is likely that the ultrarelativistic ultrahigh-energy-density plasma conditions, which are characteristic of cosmic objects, are most amply reproduced in relativistic heavy-ion collisions (see Section 5).

6.5 Matter transformation after the Big Bang

The 'most extreme' conditions, which are hard to imagine at the modern level of knowledge, undoubtedly correspond to the conditions of the Big Bang — the instant of origination of our Universe (Figs 1a and 13c). We see that elementary particle cosmology makes it possible to advance a long way in the measurement of the interaction between high-energy particles, which were of primary importance at the first instants of the life of the Universe and governed its evolution for billions of years to come. Studying the evolution of the early Universe furnishes a unique opportunity of investigating high-energy phenomena which are impossible to reproduce in a laboratory.

According to modern notions [216, 258], the temporal evolution of the Universe proceeded highly nonuniformly — being relatively slow nowadays, at the early stages it was strikingly fast, so that major qualitative changes of the state of the Universe occurred in a split second. The Universe we now observe emerged about 14 – 15 billion years ago from some initial singular state with infinitely high temperature and density, and since then it has been uninterruptedly expanding (with acceleration — as became evident quite recently) and cooling down.

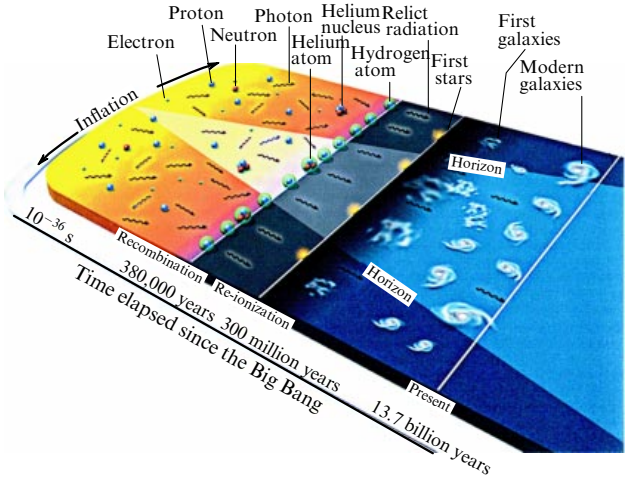

Figure 21. Temporal scale of the Universe. During inflation, the Universe expanded rapidly and the plasma, which consisted of photons and charged particles, propagated far beyond the horizon restricting the region within sight of a hypothetical observer. The onset of recombination occurred 380 thousand years later: the first atoms and the relict radiation emerged. 300 million years later, the light of the first stars ionized the major part of hydrogen and helium [259].

The enormous energies afforded by present-day accelerators are clearly insufficient for reproducing in laboratory experiments the conditions corresponding to the Grand Unification parameter range amounting to $\sim 10^{15}$ GeV. To do this would require a Solar-System-sized accelerator.

The main stages of the temporal evolution of the early Universe are presented in Fig. 21 [216, 258, 259].

The instant of the Universe's origin is the epoch of the birth of classical space–time. Generally accepted at the present time is the theory of the Big Bang, i.e., the origination of the Universe from a singularity (from spatio–temporal foam, as is sometimes said) [258]. At the instant of the birth of the Universe, the substance density ρ and temperature T amounted to Planck's values: $\rho_P \sim 10^{93}$ g cm^{-3}, and $T_P \sim 10^{32}$ K; under these conditions, the gravitational interaction was compared with the rest (strong, weak, electromagnetic) interactions in strength and should therefore be considered with the inclusion of quantization.

10^{-42} seconds after the origin of the classical space–time, an inflation stage in the Universe set in [216, 258] (see Fig. 21 [259]. It was characterized by an ultimately high negative pressure $p \sim -\rho^2$, whereat the very laws of ordinary physics of gravitating systems change. The substance in this state is the source of repulsion rather than attraction.

The equation of state of substance with a negative pressure is unstable: it should be replaced with ordinary, nonnegative pressure. That is why the inflation phase of the Universe's development terminates rather quickly and the stage of ordinary matter production sets in [216].

According to Kirzhnits [226], from this point in time on, $\sim 10^{-37}$ s after the Big Bang, the Universe underwent, following Friedman, a relatively slow expansion, and its temperature and density lowered with time. The starting

temperature was about 10^{29} K, i.e., $\sim 10^{16}$ GeV, which exceeds the X- and Y-boson masses.

At the point in time approaching $\sim 10^{-33}$ s, when the temperature had lowered to 10^{14} GeV (10^{27} K) (the X- and Y-boson mass), a phase transition occurred with the emergence of a condensate of the corresponding Higgs particles.

At the point in time near 10^{-12} s, when the temperature had lowered to 10^2 GeV(10^{15} K) (the W- and Z-boson mass), there occurred the second (electroweak) phase transition with the emergence of the second condensate of those Higgs particles which are responsible for W- and Z-particle masses.

The next phase transition supposedly took place at the point in time approaching 10^{-5} s, when the temperature had lowered to a value of ~ 100 MeV ($10^{11}-10^{12}$ K). This is the characteristic scale of quark–gluon interaction when quark confinement occurs; quarks may exist in a free state only in a very hot plasma with $T > 10^{11}$ K. As a result of the latter transition, the quark–gluon plasma transformed into a system of hadrons. In the early Universe, when the temperature far exceeded 10^{11} K, there were no protons and neutrons — there existed a 'quark soup'.

Modern experimental technology enables, as shown in Section 5.2, approaching precisely this range of extreme states and producing, in laboratory conditions, the QGP through collisions of nuclei accelerated to relativistic velocities. This corresponds to the states in the temporal neighborhood only a few milli- or microseconds after the Big Bang (Fig. 13c); the operation of the RHIC, LHC, FAIR, etc. accelerators will presumably permit advancing into the nanosecond temporal range.

As a result of the Universe's expansion, the temperature lowered, and quarks began to recombine forming protons and neutrons and cease to occur as independent particles in nature.

After the epoch of proton and neutron production, the subsequent evolution of the Universe led to the epoch of nucleosynthesis [$\sim 1-100$ s since the instant of the Big Bang, a temperature of $\sim 0.1-1$ MeV (10^9-10^{11} K) — the characteristic nuclear scale], when the primary nucleosynthesis occurred and the composition of the lightest substance constituents with an atomic weight $A < 5$ formed. Formed during this epoch are the primary light nuclei: ^{4}He (25 %), ^{2}H (3×10^{-5} %), ^{3}He (2×10^{-5} %), and ^{7}Li (10^{-9} %).

Interactions practically terminated when the temperature had lowered to $T = 0.7$ MeV. At that stage of the Universe's evolution, protons and neutrons existed in the free form, not combining into nuclei. Later on, when the temperature lowered to 100 keV, the majority of neutrons were bound in the production of deuterium, as well as helium and hydrogen.

The epoch of nucleosynthesis was followed by the epoch of hidden-mass domination, which sets in at about a temperature $T \sim 10^6$ K, depending on the type of hidden matter carrier. Beginning with this epoch, small perturbations ($\sim 10^{-5}$) of substance density grow, which originated at the initial stage of inflation and built up to the present time to an extent that galaxies, stars, and planets formed.

With a further decrease in temperature because of the predominance of the contribution from electromagnetic energy to the energy of the substance, the so-called radiation-dominated epoch emerged. During this epoch, the primary plasma obeyed the radiation-dominated equation of state: $p = \rho c^2/3$.

Experiments involving underground nuclear explosions [29, 64, 65, 92] yielded a plasma and photon temperatures of $\approx 10^7$ K and an energy density of 10^9 J cm^{-3}, corresponding to the states several minutes after the Big Bang, which are close to the lower boundary of the radiation-dominated regime. This predominance is no longer manifested during the epoch of 10^8-10^{10} s (other estimates suggest a time of $\sim 10^{12}$ s) ($T \sim 10^4-10^5$ K $\approx 1-10$ eV — the characteristic atomic energy scale), when the energies of electrons and nuclei are insufficiently high to overcome their electromagnetic attraction and electrons recombine with nuclei to give rise to a neutral atomic substance transparent to photons. The temperature of this epoch is quite well known from laboratory experiments: $T \sim 4500-3000$ K. After recombination, photons reached the observer virtually without interacting with the substance and make up the relict radiation. Nowadays its energy spectrum corresponds to the spectrum of a blackbody heated to $T \approx 2.75$ K. The temperature difference (~ 3000 K and ~ 3 K) arises from the fact that the Universe has expanded by about a factor of 1000 since the transparentization epoch.

One more major milestone is located between the epoch of recombination and our time — the formation of the large-scale structure of the Universe, or the formation of galaxies. At that time, the Universe as a whole continued to expand and cool down. In regions with a somewhat higher density than the average one, however, the substance expansion moderated due to the additional gravitational attraction and entered the phase of gravitational compression with a slow rotation.

Hydrogen and helium in these galaxies were compressed by gravitational forces and heated up, fostering thermonuclear fusion reactions. The evolution of stellar objects was considered in greater detail in Section 6.1.

The subsequent stages are inherently local and involve the Universe structure formation — the large-scale structure (clusters and superclusters) of galaxies, stars, and planets. The prevalent form of visible substance at these stages is the plasma state (cosmic plasmas — circumplanetary, interplanetary, intraplanetary plasmas, the plasmas of stars and stellar atmospheres, the plasmas of quasars and galactic nuclei, interstellar and intergalactic plasmas, and quark–gluon plasma).

At the last stages of their evolution, stars pass to the state of either a white dwarf, whose substance is an ideal ('simple') metal (a crystal lattice of nuclei surrounded by a nearly free electron gas), or a black hole, a quark or neutron star.

Therefore, we see that our Universe has gone through an extremely stormy youth full of extraordinarily striking events (Table 4). The Planck temperature $T \sim 10^{32}$ K was reached 10^{-43} seconds after the 'beginning of the world', $T = 10^{13}$ K was reached in 10^{-6} seconds, $T \sim 10^{11}$ K in 0.01 seconds, $T \sim 10^{10}$ K in 1 second, $T \sim 10^9$ K in 1 minute, $T \sim 10^4$ K (change of epochs) in 100 thousand years, and $T \sim 10^3$ K in 1 million years. The primary nucleosynthesis was completed within several minutes after the 'beginning of the world', and the formation of atoms within one million years. After this rather stormy period, the initial stage of evolution was completed and pass into routine 'senile' expansion, which we now observe approximately 15 billion years after the 'beginning of the world'.

The vigorous epochs of biological progress, of the origination of life and civilization, which we witness nowadays, are superimposed on precisely this routine development of the Universe. In particular, the planet Earth was formed about 5 billion years ago, and elementary organic life emerged about 4 billion years ago. Plants and animals emerged about 1.2 billion years ago. Early human ancestors came into

Table 4. Main epochs of the evolution of the early Universe [258].

Physical processes underlying the name of epoch	Time elapsed after the Big Bang, s	Temperature, K
Emergence of classical space–time	10^{-43}	10^{32}
Inflation	$\sim 10^{-42} - 10^{-36}$	Varies over very wide limits
Production of substance	10^{-36}	$\sim 10^{29}$
Production of a baryon excess	10^{-35}	$\sim 10^{29}$
Electroweak phase transition	10^{-10}	$\sim 10^{16} - 10^{17}$
Quark confinement	10^{-4}	$\sim 10^{12} - 10^{13}$
Primary nucleosynthesis	$1 - 200$	$\sim 10^{9} - 10^{10}$

existence about one million years ago, and the *Homo sapiens* species about 200 thousand years ago. This species began to speak only $\sim$ 50 thousand years B.C., and modern civilization is believed to have begun at the end of the last glacial period — about 10 thousand years B.C. Since then, humans have so developed that they have become capable of posing questions about the physics of extreme substance states. By the order of magnitude this time corresponds to an appraisal made by Saint Augustine in his work *The City of God* [231], who believed that civilization had originated $\sim$ 5 thousand years before. Answering the question as to what God was occupied with before creating the Universe, he said that "God was preparing hell for those who raise such questions". [231].

7. Conclusion

The science of substance structure and cosmophysics are closely related and interwoven [226]. On the one hand, the solution to almost any cosmophysical problem is unthinkable without invoking data about the substance structure of the corresponding celestial object. On the other hand, cosmophysics furnishes nuclear and subnuclear physical information which substantially supplements the data obtained in terrestrial laboratories. This applies, for instance, to the peculiarities of nuclear forces (pulsar data) and to the number of neutrino families (cosmological data). The role of space (especially of the Universe as a whole) as a source of fundamental data would be expected to rise in importance in the future as well. This is so because the limits of the potentialities of accelerator physics are already in sight. At the same time, the constantly broadening and newly emerging opportunities in experimental high-energy-density physics give hope for reproducing in laboratory conditions ultraextreme substance states, which are so typical of the past, present, and future Universe.

We conclude our exposition by demonstrating the phase diagram of a substance in the form of a sketch drawn by the hand of the genius Enrico Fermi (Fig. 22 [260]) — with only one 'experimental' point — the Sun. It only remains to wonder how much it has been possible to achieve and comprehend in a mere 50 years in the area of extreme pressures and temperatures, which are so hostile to human beings and incompatible with their life, and which at the same time are the foundation of their life.

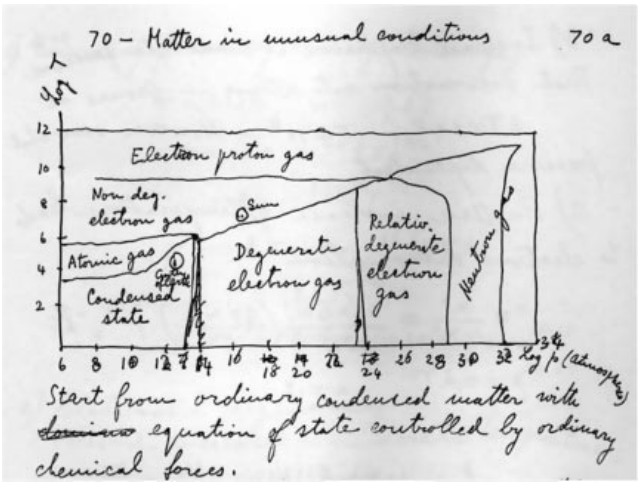

Figure 22. Phase diagram of a substance depicted by Enrico Fermi [260].

References

1. Kirzhnits D A *Usp. Fiz. Nauk* **104** 489 (1971) [*Sov. Phys. Usp.* **14** 512 (1972)]
2. Fortov V E *Usp. Fiz. Nauk* **177** 347 (2007) [*Phys. Usp.* **50** 333 (2007)]
3. Fortov V, Iakubov I, Khrapak A *Physics of Strongly Coupled Plasma* (Oxford: Oxford Univ. Press, 2006)
4. Fortov V E, Khrapak A G, Yakubov I T *Fizika Neideal'noi Plazmy* (Physics of Nonideal Plasma) (Moscow: Fizmatlit, 2004)
5. *Frontiers in High Energy Density Physics*: *The X-Games of Contemporary Science* (Washington, DC: National Acad. Press, 2003)
6. Ginzburg V L *Usp. Fiz. Nauk* **174** 1240 (2004) [*Phys. Usp.* **47** 1155 (2004)]
7. Ginzburg V L O *Fizike i Astrofizike* 3rd ed. (Moscow: Byuro Kvantum, 1995) [Translated into English: *The Physics of a Lifetime* (Berlin: Springer, 2001)]
8. Zasov A V, Postnov K A *Obshchaya Astrofizika* (General Astrophysics) (Fryazino: Vek 2, 2006)
9. Drake R P *High-Energy-Density Physics* (Berlin: Springer, 2006)
10. Vacca J R *The World's 20 Greatest Unsolved Problems* (Upper Saddle River, NJ: Prentice Hall PTR, 2005)
11. Fortov V E et al. *Zh. Eksp. Teor. Fiz.* **124** 288 (2003) [*JETP* **97** 259 (2003)]
12. Nellis W J *Rep. Prog. Phys.* **69** 1479 (2006)
13. Hammel B A, and the National Ignition Campaign Team *Plasma Phys. Control. Fusion* **48** (12B) B497 (2006)
14. Anisimov S I, Prokhorov A M, Fortov V E *Usp. Fiz. Nauk* **142** 395 (1984) [*Sov. Phys. Usp.* **27** 181 (1984)]
15. Knudson M D et al. *Phys. Rev. Lett.* **87** 225501 (2001)
16. Grabovskii E V et al. *Pis'ma Zh. Eksp. Teor. Fiz.* **60** 3 (1994) [*JETP Lett.* **60** 1 (1994)]
17. Titus Lucretius Carus *O Prirode Veshchei* (On the Nature of Things) (Series Great Thinkers) (Moscow: Mir Knigi, 2006); Lucretius *The Nature of Things* (Berkeley: Univ. of California Press, 2008)
18. Ashcroft N W, in *High Pressure Phenomena* (Eds R J Hemley et al.) (Amsterdam: IOS Press, 2002) p. 151
19. Kirzhnits D A, Lozovik Yu E, Shpatakovskaya G V *Usp. Fiz. Nauk* **117** 3 (1975) [*Sov. Phys. Usp.* **18** 649 (1975)]
20. Fortov V E (Ed.-in-Chief) *Entsiklopediya Nizkotemperaturnoi Plazmy* (Encyclopedia of Low-Temperature Plasma) (Moscow: Nauka, 2000)
21. Hemley R J, Mao H K, in *High Pressure Phenomena* (Eds R J Hemley et al.) (Amsterdam: IOS Press, 2002) p. 3
22. Fortov V E *Moshchnye Udarnye Volny i Ekstremal'nye Sostoyaniya Veshchestva* (Intense Shock Waves and Extreme States of Substance) (Moscow: Bukos, 2005)
23. Kruer W L *The Physics of Laser Plasma Interactions* (Redwood City, Calif.: Addison-Wesley, 1988)
24. Atzeni S, Meyer-ter-Vehn J *The Physics of Inertial Fusion* (Oxford: Clarendon Press, 2004)

25. Lindl J D *Inertial Confinement Fusion* (New York: Springer, 1998)
26. Pukhov A *Rep. Prog. Phys.* **66** 47 (2003)
27. Mourou G A, Tajima T, Bulanov S V *Rev. Mod. Phys.* **78** 309 (2006)
28. Hogan W J (Ed.) *Energy from Inertial Fusion* (Vienna: IAEA, 1995)
29. Avrorin E N, Vodolaga B K, Simonenko V A, Fortov V E *Usp. Fiz. Nauk* **163** (5) 1 (1993) [*Phys. Usp.* **36** 337 (1993)]
30. Caldirola P, Knoepfel H (Eds) *Physics of High Energy Density* (New York: Academic Press, 1971) [Translated into Russian (Moscow: Mir, 1974)]
31. Chen F F *Introduction to Plasma Physics and Controlled Fusion* 2nd ed. (New York: Plenum Press, 1984)
32. Al'tshuler L V, Krupnikov K K, Fortov V E, Funtikov A I *Vestn. Ross. Akad. Nauk* **74** 1011 (2004) [*Herald Russ. Acad. Sci.* **74** 613 (2004)]
33. Fortov V E, Al'tshuler L V, Trunin R F, Funtikov A I (Eds) *High-Pressure Shock Compression of Solids VII* (New York: Springer-Verlag, 2004)
34. Maksimov E G, Magnitskaya M V, Fortov V E *Usp. Fiz. Nauk* **175** 793 (2005) [*Phys. Usp.* **48** 761 (2005)]
35. Al'tshuler L V et al. *Usp. Fiz. Nauk* **169** 323 (1999) [*Phys. Usp.* **42** 261 (1999)]
36. Al'tshuler L V et al. *Usp. Fiz. Nauk* **85** 197 (1965) [*Sov. Phys. Usp.* **8** 52 (1965)]
37. Filinov V S, Levashov P R, Bonitz M, Fortov V E *Fiz. Plazmy* **31** 760 (2005) [*Plasma Phys. Rep.* **31** 700 (2005)]
38. Filinov V S et al. *J. Phys. A* **36** 6069 (2003)
39. Bezkrovniy V et al. *Phys. Rev. E* **70** 057401 (2004)
40. Fortov V E et al. *Phys. Rep.* **421** 1 (2005)
41. Loubeyre P, Occelli F, Le Toullec R *Nature* **416** 613 (2002)
42. Zel'dovich Ya B, Raizer Yu P *Fizika Udarnykh Voln i Vysokotemperaturnykh Gidrodinamicheskikh Yavlenii* (Physics of Shock Waves and High-Temperature Hydrodynamic Phenomena) 2nd ed. (Moscow: Nauka, 1966) [Translated into English (Mineola, NY: Dover Publ., 2002)]
43. Fortov V E et al. *Usp. Fiz. Nauk* **174** 495 (2004) [*Phys. Usp.* **47** 447 (2004)]
44. Dubin D H E, O'Neil T M *Rev. Mod. Phys.* **71** 87 (1999)
45. Okun L B *Leptony i Kvarki* (Leptons and Quarks) 2nd ed. (Moscow: Nauka, 1990) [Translated into English (Amsterdam: North-Holland, 1984)]
46. Okun L B *Leptony i Kvarki* (Leptons and Quarks) (Moscow: Nauka, 1981) [Translated into English (Amsterdam: North-Holland, 1982)]
47. Rubakov V A *Usp. Fiz. Nauk* **171** 913 (2001) [*Phys. Usp.* **44** 871 (2001)]
48. Schätz T, Schramm U, Habs D *Nature* **412** 717 (2001)
49. Schramm U et al. *J. Phys. B* **36** 561 (2003)
50. Pieranski P *Contemp. Phys.* **24** 25 (1983)
51. Russel W B, Saville D A, Schowalter W R *Colloidal Dispersions* (Cambridge: Cambridge Univ. Press, 1989)
52. Murray C A, Wenk R A, in *Strongly Coupled Plasma Physics* (Eds H Van Horn, S Ichimaru) (Rochester, NY: Univ. of Rochester Press, 1993) p. 367
53. Shashkin A A *Usp. Fiz. Nauk* **175** 139 (2005) [*Phys. Usp.* **48** 129 (2005)]
54. Fortov V E et al. *Phys. Rev. Lett.* **99** 185001 (2007)
55. Konyukhov A V et al. *Zh. Eksp. Teor. Fiz.* **125** 927 (2004) [*JETP* **98** 811 (2004)]
56. Fortov V *Intense Shock Waves and Extreme States of Matter* (Moscow: Bukos, 2005)
57. Clark E L et al. *Phys. Rev. Lett.* **84** 670 (2000)
58. Maksimchuk A et al. *Phys. Rev. Lett.* **84** 4108 (2000)
59. Mackinnon A J et al. *Phys. Rev. Lett.* **86** 1769 (2001)
60. Ryutov D D et al. *Phys. Plasmas* **8** 1804 (2001)
61. Burke D L et al. *Phys. Rev. Lett.* **79** 1626 (1997)
62. Faber T E *Fluid Dynamics for Physicists* (Cambridge: Cambridge Univ. Press, 1995)
63. Bamber C et al. *Phys. Rev. D* **60** 092004 (1999)
64. Vladimirov A S et al. *Pis'ma Zh. Eksp. Teor. Fiz.* **39** 69 (1984) [*JETP Lett.* **39** 82 (1984)]
65. Avrorin E N, Simonenko V A, Shibarshov L I *Usp. Fiz. Nauk* **176** 449 (2006) [*Phys. Usp.* **49** 432 (2006)]
66. Moses E I et al. *Eur. Phys. J. D* **44** 215 (2007)
67. Cavailler C *Plasma Phys. Control. Fusion* **47** B389 (2005)
68. Giorla J et al. *Plasma Phys. Control. Fusion* **48** B75 (2006)
69. Andre M, Conceptual Design of the French LMJ Laser (Monteray, 1999) p. 39
70. Spielman R B et al. *Phys. Plasmas* **5** 2105 (1998)
71. Cuneo M E et al. *Plasma Phys. Control. Fusion* **48** R1 (2006)
72. Quintenz J P, and Sandia's Pulsed Power Team, in *13th Intern. Conf. on High-Power Particle Beams, Nagaoka, Japan, June 2000*
73. Sharkov B Yu (Ed.) *Yadernyi Sintez s Inertsionnym Uderzhaniem* (Inertial Confinement Nuclear Fusion) (Moscow: Fizmatlit, 2005)
74. Fortov V E, Hoffmann D H H, Sharkov B Yu *Usp. Fiz. Nauk* **178** 113 (2008) [*Phys. Usp.* **51** 109 (2008)]
75. Belyaev V S et al. *Usp. Fiz. Nauk* **178** 823 (2008) [*Phys. Usp.* **51** 793 (2008)]
76. Reinovsky R E et al. *AIP Conf. Proc.* **706** 1191 (2004)
77. Atlas project, LASL
78. Wikipedia, Iskra laser, http://en.wikipedia.org/wiki/ISKRA_laser#iskra-6
79. Sansone G et al. *Science* **314** 443 (2006)
80. Ditmire T et al. *Phys. Rev. A* **57** 369 (1998)
81. Boehler R *Nature* **363** 534 (1993)
82. Boehler R, Forzandonea D, in *High Pressure Phenomena* (Eds R J Hemley et al.) (Amsterdam: IOS Press, 2002) p. 55
83. Loubeyre P et al. *High Pressure Res.* **24** 25 (2004)
84. Zhernokletov M V, Zubarev V N, Trunin R F, Fortov V E *Experimental'nye Dannye po Udarnoi Szhimaemosti i Adiabaticheskomu Rasshireniyu Kondensirovannykh Veshchestv pri Vysokikh Plotnostyakh Energii* (Experimental Data on Shock Compressibility and Adiabatic Expansion of Condensed Matter at High Energy Densities) (Chernogolovka: IKhF RAN, 1996)
85. Bazanov O V et al. *Teplofiz. Vys. Temp.* **23** 976 (1985) [*High Temp.* **23** 781 (1985)]
86. Hawke P S et al. *Phys. Rev. Lett.* **41** 994 (1978)
87. Pavlovski A I et al., in *Megagauss Technology and Pulsed Power Applications* (Eds C M Fowler, R S Caird, D J Erickson) (New York: Plenum Press, 1987) p. 255
88. Gryaznov V K et al. *Zh. Eksp. Teor. Fiz.* **114** 1242 (1998) [*JETP* **87** 678 (1998)]
89. Gryaznov V K et al. *Khim. Fiz.* **17** (2) 33 (1998)
90. Zhernokletov M V *Teplofiz. Vys. Temp.* **36** (2) 231 (1998)
91. Al'tshuler L V et al. *Usp. Fiz. Nauk* **166** 575 (1996) [*Phys. Usp.* **39** 539 (1996)]
92. Trunin R F *Usp. Fiz. Nauk* **164** 1215 (1994) [*Phys. Usp.* **37** 1123 (1994)]
93. Trunin R F et al. *Zh. Eksp. Teor. Fiz.* **62** 1043 (1972) [*Sov. Phys. JETP* **35** 550 (1972)]
94. Lebedev S V, Savvatimskii A I *Usp. Fiz. Nauk* **144** 215 (1984) [*Sov. Phys. Usp.* **27** 749 (1984)]
95. Zel'dovich Ya B, Landau L D *Zh. Eksp. Teor. Fiz.* **14** 32 (1944); Landau L D, Zeldovich Ya B *Acta Phys. Chem. USSR* **18** 194 (1943)
96. Turchi P J, Baker W L *J. Appl. Phys.* **44** 4936 (1973)
97. Gasilov V A, Zakharov S V, Smirnov V P *Pis'ma Zh. Eksp. Teor. Fiz.* **53** 83 (1991) [*JETP Lett.* **53** 85 (1991)]
98. Glidden S C et al., in *9th IEEE Intern. Pulsed Power Conf., Albuquerque, New Mexico, USA, June 21–23, 1993*: *Digest of Technical Papers* Vol. 1 (Eds K R Prestwich, W L Baker) (New York: IEEE, 1993) p. 459
99. Chittenden J P et al. *Phys. Rev. Lett.* **98** 025003 (2007)
100. Ryutov D D, Derzon M S, Matzen M K *Rev. Mod. Phys.* **72** 167 (2000)
101. Mokhov V N, in *Megagauss-IX*: *Proc. of 9th Intern. Conf. on Megagauss Magnetic Field Generation and Related Topics, 2002, Moscow, St. Petersburg, Russia* (Eds V D Selemir, L N Plyashkevich) (Sarov: VNIIEF, 2004) p. 665
102. Fortov V E (Ed.) *Explosive-Driven Generators of Powerful Electrical Current Pulses* (Cambridge: Cambridge Int. Sci. Publ. Ltd, 2007)
103. Boyko B A et al., in *Megagauss Magnetic Field Generation, Its Application to Science and Ultra-High Pulsed-Power Technology*: *Proc. VIIIth Intern. Conf. Megagauss Magnetic Field Generation and Related Topics, Tallahassee, Florida, USA, 18–23 October 1998* (Ed. H J Schneider-Muntau) (Hackensack, NJ: World Scientific, 2004) p. 61
104. Azizov E A et al. *AIP Conf. Proc.* **651** 29 (2002)

105. Glushkin V A et al., in *BEAMS'98*: *Proc. 12th Intern. Conf. on High-Power Particle Beams, June 7 – 12, 1998, Haifa, Izrael, 1998* (Eds M Markonits, J Shiloh) (Piscataway, NJ: IEEE, 1998) p. 71
106. Selemir V D et al., in *Megagauss-X, Berlin, 2004* (Ed. M von Ortenberg) (Berlin: Humboldt Univ., 2005) p. 219
107. Mourou G A, Barry C P J, Perry M D *Phys. Today* **51** (1) 22 (1998)
108. Bahk S-W et al. *Opt. Lett.* **29** 2837 (2004)
109. Bulanov S V *Plasma Phys. Control. Fusion* **48** (12B) B29 (2006)
110. MAGPIE, http://dorland.pp.ph.ic.ac.uk/magpie/
111. Unruh W G *Phys. Rev. D* **14** 870 (1976)
112. Schützhold R, Schaller G, Habs D *Phys. Rev. Lett.* **97** 121302 (2006)
113. Chen P, Tajima T *Phys. Rev. Lett.* **83** 256 (1999)
114. Strickland D, Mourou G *Opt. Commun.* **56** 219 (1985)
115. Strickland D, Mourou G *Opt. Commun.* **55** 447 (1985)
116. Maine P, Mourou G *Opt. Lett.* **13** 467 (1988)
117. Maine P et al. *IEEE J. Quantum Electron.* **24** 398 (1988)
118. Bunkenberg J et al. *IEEE J. Quantum Electron.* **17** 1620 (1981)
119. Bula C et al. *Phys. Rev. Lett.* **76** 3116 (1996)
120. Telnov V *Nucl. Instrum. Meth. Phys. Res. A* **472** 43 (2001)
121. Benuzzi-Mounaix A et al. *Plasma Phys. Control. Fusion* **48** (12B) B347 (2006)
122. Pukhov A, Meyer-ter-Vehn J *Appl. Phys. B* **74** 355 (2002)
123. Beg F N et al. *Phys. Plasmas* **4** 447 (1997)
124. Norreys P A et al. *Phys. Plasmas* **6** 2150 (1999)
125. Sarkisov G S et al. *Phys. Rev. E* **59** 7042 (1999)
126. Bulanov S V, Naumova N M, Pegoraro F *Phys. Plasmas* **1** (3) 745 (1994)
127. Kodama R et al. *Phys. Rev. Lett.* **84** 674 (2000)
128. Mangles S P D et al. *Nature* **431** 535 (2004)
129. Maksimchuk A et al. *Fiz. Plazmy* **30** 514 (2004) [*Plasma Phys. Rep.* **30** 473 (2004)]
130. Esirkepov T, Yamagiwa M, Tajima T *Phys. Rev. Lett.* **96** 105001 (2006)
131. Disdier L et al. *Phys. Rev. Lett.* **82** 1454 (1999)
132. Gahn C et al. *Appl. Phys. Lett.* **77** 2662 (2000)
133. Esirkepov T Zh et al. *Phys. Rev. Lett.* **89** 175003 (2002)
134. Mima K et al. *Phys. Rev. Lett.* **57** 1421 (1986)
135. Burke D L et al. *Phys. Rev. Lett.* **79** 1626 (1997)
136. Tatarakis M et al. *Nature* **415** 280 (2002)
137. Mason R J, Tabak M *Phys. Rev. Lett.* **80** 524 (1998)
138. Nakajima K et al. *Phys. Rev. Lett.* **74** 4428 (1995)
139. Malka V et al. *Science* **298** 1596 (2002)
140. Kanel G I, Razorenov S V, Fortov V E *Shock-Wave Phenomena and Properties of Condensed Matter* (New York: Springer, 2004)
141. Rubakov V A, Shaposhnikov M E *Phys. Lett. B* **125** 136 (1983)
142. Arkani-Hamed N, Dimopoulos S, Dvali G *Phys. Rev. D* **59** 086004 (1999)
143. Giddings S B, Thomas S *Phys. Rev. D* **65** 056010 (2002)
144. Rubakov V A *Usp. Fiz. Nauk* **173** 219 (2003) [*Phys. Usp.* **46** 211 (2003)]
145. Zel'dovich Ya B, Popov V S *Usp. Fiz. Nauk* **105** 403 (1971) [*Sov. Phys. Usp.* **14** 673 (1972)]
146. Hawking S W *Commun. Math. Phys.* **43** 199 (1975)
147. Parker L *Phys. Rev.* **183** 1057 (1969)
148. Shearer J W et al. *Phys. Rev. A* **8** 1582 (1973)
149. Mima K *AIP Conf. Proc.* **740** 387 (2004)
150. Liang E P, Wilks S C, Tabak M *Phys. Rev. Lett.* **81** 4887 (1998)
151. Narozhny N B et al. *Phys. Lett. A* **330** 1 (2004)
152. Galy J et al. *New J. Phys.* **9** 23 (2007)
153. Schwoerer H et al. *Europhys. Lett.* **61** 47 (2003)
154. Ledingham K W D et al. *Phys. Rev. Lett.* **84** 899 (2000)
155. Umstadter D *Nature* **404** 239 (2000)
156. Malka G et al. *Phys. Rev. E* **66** 066402 (2002)
157. Magill J et al. *Appl. Phys. B* **77** 387 (2003)
158. Ledingham K W D, McKenna P, Singhal R P *Science* **300** 1107 (2003)
159. Chiu C et al. *Med. Phys.* **31** 2042 (2004)
160. Leemans W P et al. *Phys. Plasmas* **8** 2510 (2001)
161. Cowan T E et al. *Phys. Rev. Lett.* **84** 903 (2000)
162. Tajima T *AIP Conf. Proc.* **569** 77 (2001)
163. Fujiwara M, Kawase K, Titov A T *AIP Conf. Proc.* **802** 246 (2005)
164. Novikov I D *Usp. Fiz. Nauk* **171** 859 (2001) [*Phys. Usp.* **44** 817 (2001)]
165. Karsch F *AIP Conf. Proc.* **842** 20 (2006)
166. Rubakov V A *Usp. Fiz. Nauk* **177** 407 (2007) [*Phys. Usp.* **50** 390 (2007)]
167. Riordan M, Zajc W A *Sci. Am.* **294** (5) 35 (2006); *V Mire Nauki* (8) 21 (2006)
168. Gyulassy M, McLerran L *Nucl. Phys. A* **750** 30 (2005)
169. Langanke K, in *A FAIR Chance for Nuclear Astrophysics, Kick-Off Event and Symp. on the Physics at FAIR, November 7 – 8, 2007*
170. Hoffmann D H H et al. *Phys. Plasmas* **9** 3651 (2002)
171. Baumung K et al. *Laser Part. Beams* **14** 181 (1996)
172. Mesyats G A *Impul'snaya Energetika i Elektronika* (Pulsed Energetics and Electronics) (Moscow: Nauka, 2004)
173. Fortov V, Rudakov L, Ni A *Sov. Technol. Rev. B* **371** 589 (1992)
174. Kanel' G I, Razorenov S V, Utkin A V, Fortov V E *Udarno-Volnovye Yavleniya v Kondensirovannykh Sredakh* (Shock-Wave Phenomena in Condensed Media) (Moscow: Yanus-K, 1996)
175. Kanel' G I, Fortov V E, Razorenov S V *Usp. Fiz. Nauk* **177** 809 (2007) [*Phys. Usp.* **50** 771 (2007)]
176. Rosmej O N et al. *Phys. Rev. A* **72** 052901 (2005)
177. Efremov V P et al. *Pis'ma Zh. Eksp. Teor. Fiz.* **81** 468 (2005) [*JETP Lett.* **81** 378 (2005)]
178. Mintsev V et al. *Contrib. Plasma Phys.* **39** 45 (1999)
179. Tahir N A et al. *Contrib. Plasma Phys.* **45** 229 (2005)
180. Tahir N A et al. *Phys. Rev. Lett.* **95** 035001 (2005)
181. Mrówczyński S, Thoma M H *Annu. Rev. Nucl. Part. Sci.* **57** 61 (2007)
182. Hands S *Contemp. Phys.* **42** (4) 209 (2001)
183. Glendenning N K *Compact Stars*: *Nuclear Physics, Particle Physics, and General Relativity* 2nd ed. (New York: Springer, 2000)
184. Shuryak E V *Phys. Rep.* **61** 71 (1980)
185. Shuryak E V *Phys. Lett. B* **78** 150 (1978)
186. Kalashnikov O K, Klimov V V *Phys. Lett. B* **88** 328 (1979)
187. Kapusta J I *Nucl. Phys. B* **148** 461 (1979)
188. Collins J C, Perry M J *Phys. Rev. Lett.* **34** 1353 (1975)
189. Baym G, Chin S A *Phys. Lett. B* **62** 241 (1976)
190. Freedman B A, McLerran L D *Phys. Rev. D* **16** 1169 (1977)
191. Chapline G, Nauenberg M *Phys. Rev. D* **16** 450 (1977)
192. Adams J et al. (STAR Collab.) *Phys. Rev. Lett.* **92** 062301 (2004)
193. Sorensen P R, PhD Thesis (Los Angeles, Calif.: Univ. of California, 2003); nucl-ex/0309003
194. Adams J et al. (STAR Collab.) *Phys. Rev. Lett.* **92** 052302 (2004)
195. Adler S S et al. (PHENIX Collab.) *Phys. Rev. Lett.* **91** 182301 (2003)
196. Alt C et al. *Phys. Rev. C* **68** 034903 (2003)
197. Baym G "Matter under extreme conditions", July 2007
198. Gyulassy M, Plümer M *Nucl. Phys. A* **527** 641 (1991)
199. Gyulassy M et al. *Nucl. Phys. A* **538** 37 (1992)
200. Wang X-N, Gyulassy M *Phys. Rev. Lett.* **68** 1480 (1992)
201. Stöcker H et al. *Prog. Part. Nucl. Phys.* **4** 133 (1980)
202. Gyulassy M "Quark gluon plasmas: Femto cosmology with A + A @ LHC", July 2008
203. Cherepashchuk A M, Chernin A D *Vselennaya, Zhizn', Chernye Dyry* (Universe, Life, Black Holes) (Fryazino: Vek-2, 2004)
204. Lyutikov M *Mon. Not. R. Astron. Soc.* **367** 1594 (2006)
205. Leemans W P et al. *Phys. Plasmas* **11** 2899 (2004)
206. Takabe H, in *Edward Teller Lectures* (Eds M Hora, G H Miley) (Sydney: Univ. South Sydney, 2004) p. 331
207. Nellis J W, in *High Pressure Phenomena* (Eds R J Hemley et al.) (Amsterdam: IOS Press, 2002) p. 607
208. Balega Yu Yu *Usp. Fiz. Nauk* **172** 945 (2002) [*Phys. Usp.* **45** 883 (2002)]
209. Allard F et al. *Annu. Rev. Astron. Astrophys.* **35** 137 (1997)
210. Chabrier G, Baraffe I *Annu. Rev. Astron. Astrophys.* **38** 337 (2000)
211. Koester D *Astron. Astrophys. Rev.* **11** (1) 33 (2002)
212. Rebolo R, Martin E L, Zapatero Osorio M R (Eds) *Brown Dwarfs and Extrasolar Planets* (San Francisco, Calif.: Astron. Soc. of the Pacific, 1998)
213. Klumov B A et al. *Usp. Fiz. Nauk* **164** 617 (1994) [*Phys. Usp.* **37** 577 (1994)]
214. Fortov V E et al. *Usp. Fiz. Nauk* **166** 391 (1996) [*Phys. Usp.* **39** 363 (1996)]
215. Kaplan S A *Fizika Zvezd* (The Physics of Stars) 2nd ed. (Moscow: Nauka, 1970) [Translated into English (Chichester: Wiley, 1982)]

216. Rubin S G *Ustroistvo Nashei Vselennoi* (The Constitution of Our Universe) (Fryazino: Vek 2, 2006)
217. Levin A *Populyarnaya Mekh*. (8) 38 (2007)
218. HUBBLESITE, http://hubblesite.org/
219. Mezzacappa A *Annu. Rev. Nucl. Part. Sci.* **55** 467 (2005)
220. Rodionova Zh F, Surdin V G, in *Astronomiya: Vek XXI* (Astronomy: XXIst Century) (Ed.-Compiler V G Surdin) (Fryazino: Vek 2, 2007) p. 34
221. Shevchenko V V, in *Sovremennoe Estestvoznanie. Entsiklopediya* (Modern Natural Science. Encyclopedia) (Ed. V N Soifer) (Moscow: Nauka, 1999)
222. Gelliot T, 2007 (private communication)
223. Yakovlev D G, Levenfish K P, Shibanov Yu A *Usp. Fiz. Nauk* **169** 825 (1999) [*Phys. Usp.* **42** 737 (1999)]
224. Haensel P, Potekhin A Y, Yakovlev D G *Neutron Stars 1*: *Equation of State and Structure* (New York: Springer, 2007)
225. Shapiron S L, Teukolsky S A *Black Holes, White Dwarfs, and Neutron Stars* (New York: Wiley, 1983) [Translated into Russian (Moscow: Mir, 1985)]
226. Kirzhnits D A *Lektsii po Fizike* (Lectures on Physics) (Moscow: Nauka, 2006)
227. Istomin Ya N *Usp. Fiz. Nauk* **178** 880 (2008) [*Phys. Usp.* **51** 844 (2008)]
228. Page D, Applegate J H *Astrophys. J. Lett.* **394** L17 (1992)
229. Kouveliotou C, Duncan R, Thompson C, in *Kosmos*: *Vselennaya, Galaktiki, Zvezdy, Planety: Al'manakh* (Cosmos: Universe, Galaxies, Stars, Planets: Miscellany) (Ed.-Compiler V G Surdin) (Moscow: V Mire Nauki, 2006) p. 134
230. Cherepashchuk A M *Usp. Fiz. Nauk* **166** 809 (1996) [*Phys. Usp.* **39** 759 (1996)]
231. Hawking S W A *Brief History of Time*: *from the Big Bang to Black Holes* (Toronto: Bantam Books, 1988) [Translated into Russian (St. Petersburg: Amfora, 2007)]
232. Karnakov B M, Mur V D, Popov V S *Pis'ma Zh. Eksp. Teor. Fiz.* **65** 391 (1997) *[JETP Lett.* **65** 405 (1997)]
233. Popov V S, Karnakov B M, Mur V D *Phys. Lett. A* **229** 306 (1997)
234. Kardashev N S, Novikov I D, Shatskii A A *Astron. Zh.* **83** 675 (2006) [*Astron. Rep.* **50** 601 (2006)]
235. Shinkai H, Hayward S A *Phys. Rev. D* **66** 044005 (2002)
236. Lobo F S N *Phys. Rev. D* **71** 084011 (2005)
237. Panasyuk M I *Stranniki Vselennoi ili Ekho Bol'shogo Vzryva* (Wanderers of the Universe or the Big Bang Echo) (Fryazino: Vek 2, 2005)
238. Fabrika S *Astrophys. Space Phys. Rev.* **12** 1 (2004)
239. Willingale L et al. *Phys. Rev. Lett.* **96** 245002 (2006)
240. Kando M et al. *J. Nucl. Mater.* **248** 405 (1997)
241. Surdin V G *Rozhdenie Zvezd* (Star Production) (Moscow: Editorial URSS, 1999)
242. Aschwanden M J *Physics of the Solar Corona*: *An Introduction with Problems and Solutions* (Berlin: Springer, 2006) p. 869
243. Nishida A *Space Sci. Rev.* **91** 507 (2000)
244. Zelenyi L M et al. *Usp. Fiz. Nauk* **175** 643 (2005) [*Phys. Usp.* **48** 615 (2005)]
245. Ayukov S V et al. *Pis'ma Zh. Eksp. Teor. Fiz.* **80** 163 (2004) [*JETP Lett.* **80** 141 (2004)]
246. Greisen K *Phys. Rev. Lett.* **16** 748 (1966)
247. Surdin V G, in *Astronomiya*: *Vek XXI* (Astronomy: XXIst Century) (Ed.-Compiler V G Surdin) (Fryazino: Vek 2, 2007) p. 267
248. Meszaros P, Rees M J *Astrophys. J.* **405** 278 (1993)
249. Price P A et al. *Astrophys. J.* **572** L51 (2002)
250. Blinnikov S I et al. *Pis'ma Astron. Zh.* **10** 422 (1984) [*Sov. Astron. Lett.* **10** 177 (1984)]
251. Kodama R et al. *Nature* **412** 798 (2001)
252. Sunyaev R A, Zeldovich Ya B *Nature* **223** 721 (1969)
253. Zel'dovich Ya B, Levich E V, Syunyaev R A *Zh. Eksp. Teor. Fiz.* **62** 1392 (1972) [*Sov. Phys. JETP* **35** 733 (1972)]
254. Drake R P et al. *Phys. Plasmas* **11** 2829 (2004)
255. Arnett D *Astrophys. J.* **427** 932 (1994)
256. McCray R *Annu. Rev. Astron. Astrophys.* **31** 175 (1993)
257. Remington B A et al. *Phys. Plasmas* **4** 1994 (1997)
258. Sazhin M V, in *Sovremennoe Estestvoznanie. Entsiklopediya* (Modern Natural Science. Encyclopedia) (Ed. by V N Soifer) (Moscow: Nauka, 1999)
259. Hu W, White M, in *Kosmos*: *Vselennaya, Galaktiki, Zvezdy, Planety*: *Al'manakh* (Cosmos: Universe, Galaxies, Stars, Planets: Miscellany) (Ed.-Compiler V G Surdin) (Moscow: V Mire Nauki, 2006) p. 42
260. Fermi E "Notes on thermodynamics and statistics" (1953); *Notes on Thermodynamics and Statistics* (Chicago: Univ. of Chicago Press, 1966)
261. Waxman E *Plasma Phys. Control. Fusion* **48** (12B) B137 (2006)